An Orbital Meteoroid Stream Survey using the Southern Argentina Agile MEteor Radar (SAAMER) based on a Wavelet approach

P. Pokorný[a,*], D. Janches[b], P. G. Brown[a], J. L. Hormaechea[c]

[a]*Dept. of Physics and Astronomy, University of Western Ontario, London, Ontario, Canada N6A 3K7*
[b]*Space Weather Lab., Mail Code 674, GSFC/NASA, Greenbelt, MD 20771, United States*
[c]*Facultad de Cs. Astronomicas y Geofisicas, UNLP, y CONICET, Estacin Astronomica Rio Grande, Tierra del Fuego, Argentina*

Abstract

Over a million individually measured meteoroid orbits were collected with the Southern Argentina Agile MEteor Radar (SAAMER) between 2012–2015. This provides a robust statistical database to perform an initial orbital survey of meteor showers in the Southern Hemisphere via the application of a 3D wavelet transform. The method results in a composite year from all 4 years of data, enabling us to obtain an undisturbed year of meteor activity with more than one thousand meteors per day. Our automated meteor shower search methodology identified 58 showers. Of these showers, 24 were associated with previously reported showers from the IAU catalogue while 34 showers are new and not listed in the catalogue. Our searching method combined with our large data sample provides unprecedented accuracy in measuring meteor shower activity and description of shower characteristics in the Southern

*Corresponding author
Email address: `ppokorn2@uwo.ca` (P. Pokorný)

Preprint submitted to Icarus *November 3, 2016*

Hemisphere. Using simple modeling and clustering methods we also propose potential parent bodies for the newly discovered showers.

Keywords:

meteor showers, meteoroids streams, meteors, radar

1. Introduction

The meteoroid background as measured at Earth can be broadly divided into two components: sporadic and shower meteors (Jenniskens, 2006). Sporadic meteoroids have no specific linkage to one another or to a particular parent body while shower meteoroids exhibit a common orbit suggestive of a physical linkage among stream members (variously defined by a host of possible similarity criteria, e.g. Valsecchi et al., 1999) which suggests a common parentage, though this parent body is often unknown. The fact that shower meteors may be linked to a parent makes them particularly valuable as proxy material for understanding comets and asteroids; shower meteors are small fragments of the parents and in effect, windows into the origin and evolution of these small solar system bodies. Identification of new showers may allow indirect sampling of parent bodies not previously studied and the particle distribution, shower duration, flux profile and radiant dispersion are diagnostic of the mode and timing of parent body decay. Such physical data on streams have been variously used to constrain meteoroid stream formation and evolution models (e.g. Jenniskens et al., 2010; Wiegert and Brown, 2005).

Besides the study of specific showers, some analyses require that dynamical models are compared against all known showers, in the forms of shower catalogs. Association between predicted showers and those observed form the basis for validation of such models. For example, Babadzhanov et al. (2008a) utilized a numerical integration method to investigate the orbital evolution of the near-Earth asteroid 2003 EH_1 and showed that its orbit intersects that of the Earth at eight different points with different values of argument of perihelion ω. Since the resulting orbital parameters are different at each intersection the model explicitly predicted the existence of eight different meteor showers, presuming the complex was old enough. Using published catalogs, these theoretically predicted showers were tentatively identified with observed streams. However, better information about those streams was required to prove such association and set limits to the age of the stream complex. Clearly, establishing which showers exist and which are spurious becomes critical to validating such models. In this manner, meteor shower catalogs constrain the past orbital evolution and physical character of presently detected Near-Earth Objects (NEO; Babadzhanov et al., 2008c,b).

Establishing the very existence of a shower is often a difficult task. Particularly for weaker streams, basic physical characteristics (radiant drift, duration, mass distribution) can be challenging to measure. While several dozen strong meteor showers have been known for many decades, the majority of showers are only weakly active and require large numbers of instrumentally recorded meteor radiants to separate the shower "signal" from the much stronger sporadic background "noise". Recently, optical surveys have overcome this barrier in part by using large numbers of small cameras and automated meteor detection software to obtain multi-station radiants for large datasets (SonotaCo, 2009; Molau and Rendtel, 2009; Jenniskens et al., 2011) and in so doing have identified several probable new minor showers. Optical instruments, however, are limited to nighttime hours and clear skies - the results of such surveys will tend to show large seasonal biases. Radar observations, in contrast, are able to record independent of weather and diurnal conditions. The major limitation of radar observations in shower characterization is the lower metric precision of each measured event; however this limitation is compensated through much larger datasets, with large number statistics providing higher sensitivity for detection of weak showers.

In the last two decades several long-term optical and radar orbit survey programs have been undertaken from northern hemisphere sites most notably The Cameras for Allsky Meteor Surveillance (CAMS, Jenniskens et al., 2011) based on optical observations and a complementary survey performed with the Canadian Meteor Orbit Radar (CMOR, Brown et al., 2010, hereafter B2010) utilizing backscatter transverse radio wave scattering. In contrast, the southern hemisphere has only two recent shower surveys performed using single-station radar observations (Younger et al., 2009; Janches et al., 2013). An effort to fill this gap utilizing optical and video observations has taken place in the past few years (Bland et al., 2012; Jopek et al., 2010; Molau and Kerr, 2014; Towner et al., 2015; Jenniskens et al., 2016a), focusing on larger fireballs but which are limited by weather and day/night cycles. We note that the Advanced Meteor Orbit Radar (AMOR) which operated in Christchurch, New Zealand during the 1990s, produced some 0.5 Megaorbits, but at such small particle sizes that only half a dozen of the strongest showers were visible in the resulting dataset (Galligan and Baggaley, 2004).

In this work we report on an extension of our earlier initial single-station radar study of meteor showers using the Southern Argentina Agile MEteor Radar (SAAMER, Janches et al., 2013, hereafter J2013). In J2013 we provisionally identified showers using radar measurements of individual meteor echoes and a statistical radiant approach which exploited the specular geometry of meteor backscatter detection along the lines first proposed by Jones (1977) and developed in detail by Jones and Jones (2006).

In this study we expand on J2013 by making use of individually measured radiants/orbits (totaling ∼1 Megaorbit) collected by the Orbital System; an upgrade of SAAMER into a system capable of recording meteor orbits by adding two remote receiving stations (Janches et al., 2015, hereafter referred as SAAMER-OS). Specifically, the orbits used in this study were collected in the time period January 2012-January 2016. As first proposed by Galligan and Baggaley (2002), we make use of the wavelet transform to extract shower signals from SAAMER-OS. For this study, we apply a 3D wavelet transform to identify showers, using the same general thresholds, background definition and shower linkage approach used by B2010 for the CMOR Northern Hemisphere radar survey. However, we have developed a revised method of computing background levels which includes both statistical fluctuations and the physical background averaged throughout the year. This approach has allowed us to improve sensitivity in both localizing 3D wavelet maxima and linking them together as probable showers as compared to the original B2010 CMOR survey. We also compare common showers observed by CMOR and SAAMER-OS in an effort to cross-validate results.

Finally, we have also explicitly applied our new shower linkage algorithm in an attempt to confirm all showers listed in the International Astronomical

Union working list of meteor showers both on a year-to-year basis and in our composite single "virtual" year. Finally, we examine the probable origin and parent bodies of our newly detected showers.

2. Overview of SAAMER-OS Hardware and Detection Software

The SAAMER-Orbital System (OS), described in detail in Janches et al. (2015) is hosted by the Estacion Astronomica Rio Grande (EARG), located in Rio Grande, Tierra del Fuego, Argentina. It consists of three distinct radar stations: the central station (SAAMER-C; 53.79S, 67.75W) that hosts the transmitting and interferometry-enabled receiving antenna arrays, the northern remote station (SAAMER-N; 53.68S, 67.87W) located approximately 13 km northwest of the central station, and the western remote station (SAAMER-W; 53.83S, 67.84W) located approximately 8 km southwest of the central station. SAAMER-C has been in operation since May 2008 and utilizes high peak transmitter power (60 kW) at a frequency of 32.55 MHz. Together with a relatively narrow beam pattern provided by an eight-antenna transmitter array comprised of 3-element crossed yagi antennas (Fritts et al., 2010, J2013) this allows detection of smaller meteoroids relative to most specular all-sky meteor radars (which have peak transmit powers of 6-20 kW; W. Hocking Personal Communication, 2015 and Fritts et al., 2012). The transmitting array is organized in a circular pattern of diameter 27.6 m (i.e., 3 times the radar wavelength) and the phase differences among transmitting antennas can be changed electronically, adding flexibility to the system to perform a number of transmitting and receiving modes (Janches et al., 2014). In normal operation mode each transmitting antenna transmits at a phase difference of 180° from the adjoining two antennas (i.e. every other antenna has the same phase), providing a gain pattern in which the majority of the power is focused into eight beams at 45° azimuth increments with peak power at approximately 35° zenith. The resulting transmit gain pattern results in the majority of meteor echo detections to occur between zenith angles of 15° and 50°. Details of the system parameters utilized for the different modes of operation can be found in Janches et al. (2013, 2014, 2015).

The limiting magnitude of SAAMER-OS appears to be close to radio magnitude +11 for single station observations, while the median magnitude for orbital system requiring data from at least two remote stations is likely closer to +9.5. Equivalent mass for orbital echoes from Verniani (1973) at 30 km s^{-1} is 10^{-8} kg (or 300 microns in diameter). This is an order of magnitude in mass smaller than CMOR orbital masses (B2010).

A receiving antenna array with interferometry capability is also located at SAAMER-C. The array is a typical configuration for meteor radar systems consisting of 5 antennas, each of which is a 3-element vertically directed crossed yagi (Hocking et al., 1997). The two remote stations, SAAMER-N and SAAMER-W, were deployed in August 2010 to enable meteoroid orbit determination through the time of flight method (Baggaley et al., 1994) and are each equipped with a single 3-element vertically-directed crossed yagi receiving antenna. The remote stations were placed in such a way that they are in nearly orthogonal directions relative to SAAMER-C at a distance on the order of 10 km. For common meteor echoes detected by all three of the SAAMER-OS stations, the meteoroid trajectory and speed can be determined using the measured time delays between the detections combined with information from the interferometry from SAAMER-C (Baggaley et al., 1994; Webster and Jones, 2004; Brown et al., 2008). The details of how meteoroid orbits are measured are described in detail by Janches et al. (2015).

2.1. Data and Results

Figure 1 shows the daily count of determined meteoroid orbits observed throughout the survey period (January 2012-December 2015). It can be seen that the system can measure up to $\sim$ 1800 meteoroid orbits per day. Unfortunately, due to terrestrial interference during this time there are several periods in which there is lack of data preventing from the detection of weak or minor showers for this initial survey (see Janches et al., 2015, for more details). Despite this interruption, a total of 1,001,536 meteoroid orbits were measured as of December 31st, 2015 by SAAMER-OS, which represents the largest sample in the Southern Hemisphere to date (Janches et al., 2015).

Figure 2 shows the number of the determined meteoroid orbits in each one degree bin in solar longitude of an equivalent stacked or composite year. Stacking data results in loss of the temporal resolution, however, this is compensated by an increase in meteor counts in each solar longitude bin since data with many gaps may result in artifacts in the wavelet search and thus detection of non-existent meteor showers. By producing a composite year through combining the four year data set we always have more than 1000 meteor orbits per one degree bin in solar longitude.

The distribution of SAAMER-OS observed meteoroid radiants is shown in Fig. 3. The radiants are displayed in ecliptic coordinates in which they are viewed from an Earth-centered frame of reference (Jones and Brown, 1993). The figure is oriented such that the center point corresponds to the

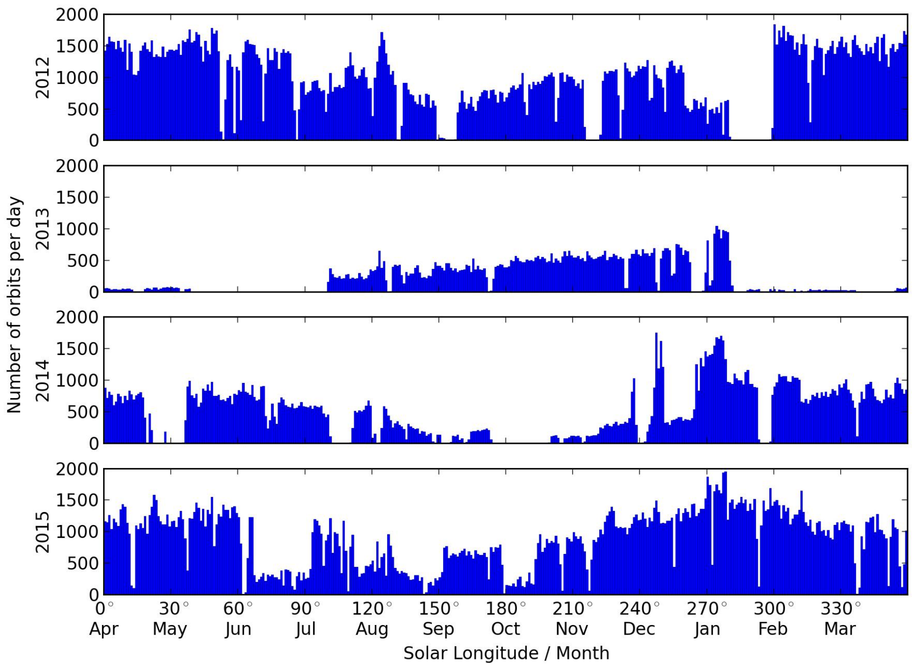

Figure 1: Number of orbits per day for the years 2012 - 2015 as recorded by SAAMER-OS. Gaps in data are due to terrestrial interference and equipment malfunctions that SAAMER experienced during this period (see Janches et al., 2015, for more details).

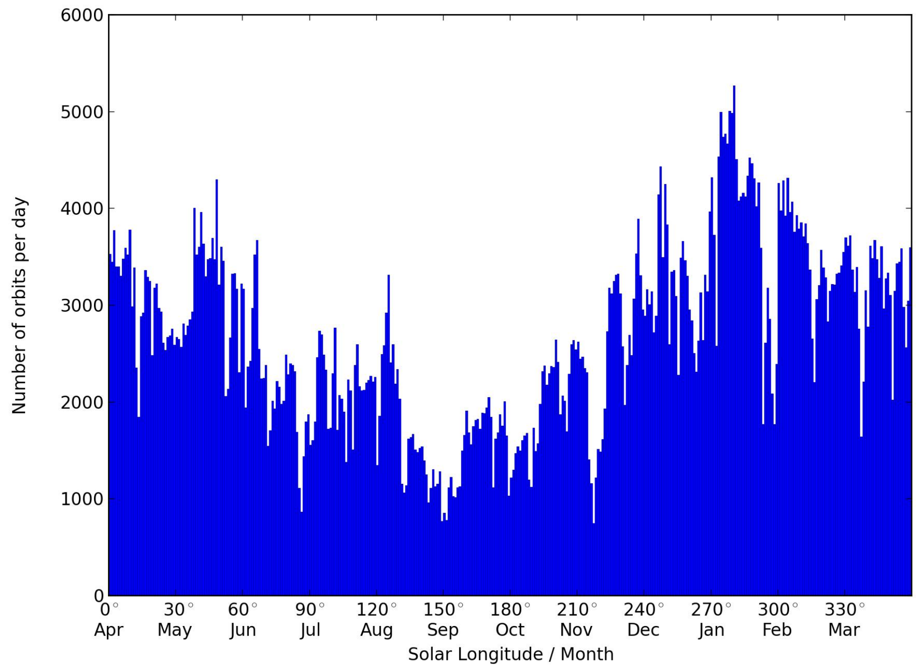

Figure 2: The same as in Fig. 1 but now all the data stacked into one virtual year. For each day in this virtual year SAAMER-OS recorded at least 1000 meteors.

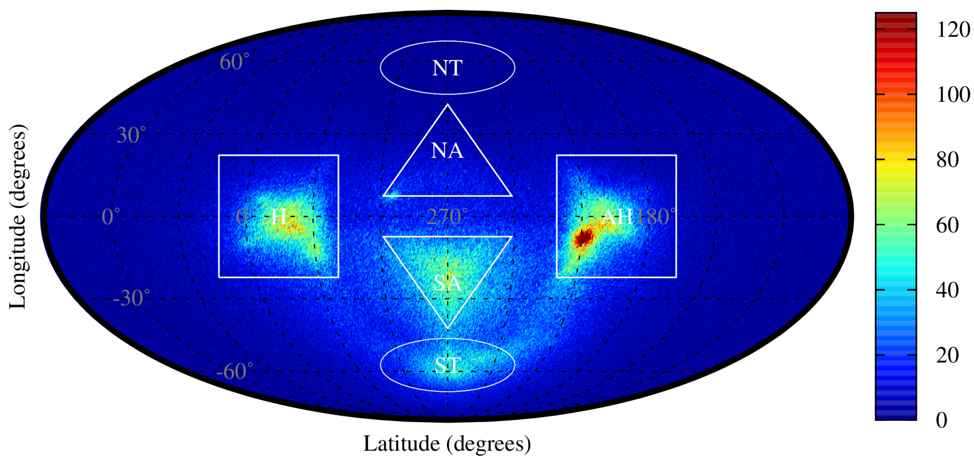

Figure 3: Raw radiant distribution of all SAAMER orbits measured over 4 consecutive years, from 2012 - 2015, with radiant density color coded in $0.5^\circ \times 0.5^\circ$ bins. We used sun-centered coordinates, where the apex of the Earth's motion is in the center of the plot, zero degrees latitude corresponds to the ecliptic plane and the sun is located at (0,0). The Helion source is to the left, the weakly visible North Apex source is in the center above the apex point, the South Apex source in the center below the ecliptic, the Antihelion source with the most prominent Southern δ Aquariids shower to the right, and the South Toroidal source at the bottom of the plot.

Apex of the Earth's way. For reference, the locations of the six sporadic meteoroid apparent sources are highlighted. These are the North and South Apex (NA/SA), the North and South Toroidal (NT/ST) and the Helion (H) and Antihelion (AH). Contributions from the sporadic apparent sources to the radiant distribution observed by SAAMER-OS are evident in this Figure, as well as 2 strong meteor showers, which appear as dense concentrated enhancements in the radiant distribution (Janches et al., 2014). The strong enhancement within the Anti Helion (AH) source corresponds to the Southern δ Aquariid (SDA) shower, which has such strong activity that it dominates the color scale in Fig. 3. The weaker enhancement to the left of the North Apex (NA) source corresponds to the Eta Aquariid shower (ETA, Campbell-Brown and Brown, 2015). As expected, the majority of meteors observed by SAAMER-OS originate from radiant locations south of the ecliptic (i.e. the ecliptic latitude of the radiant is negative), with particularly strong contributions from the South Apex (SA), South Toroidal (ST), Helion (H) and AH sources.

3. Orbit Computation

Janches et al. (2015) describes details of the meteoroid orbit measurement method used by SAAMER-OS. Briefly, when a meteor is detected at SAAMER-C, the location (i.e. range, azimuth, and elevation) of the specular reflection point on the meteor trail is determined using the interferometric receiving array (Hocking et al., 2001; Lau et al., 2006). The specular reflection point is defined as the point on the trail that minimizes the signal travel path from the transmit array to the meteor trail. It is the point at which the meteoroid is at its minimum range from the central station. At this point the meteoroid's velocity is normal to the position vector from the radar. The range ρ, elevation α, and azimuth ψ, to the specular point on the trail give the position of the meteoroid at the specular point relative to the central station using the SAAMER-C interferometric capabilities.

The meteoroid's absolute velocity is obtained from the time delay between the echo's appearance at the main site relative to the remote sites, SAAMER-N and SAAMER-W, and the known (and fixed) vector's relating the positon of SAAMER-C relative to SAAMER-N and SAAMER-W using the geometrical technique previously employed at AMOR (Baggaley et al., 1994) and CMOR (Webster and Jones, 2004; Jones et al., 2005). This geometrical method is applied to all meteors that are detected at all three SAAMER receiving stations and relies on the assumption that the interaction between the radar signal and the meteor trail is described by the specular reflection condition. This constrains the possible locations of the echo points along the trail as detected at the remote stations, which receive the forward scattered signal transmitted by SAAMER-C from (generally) different scattering points along the meteor trail. The measured time delay between each of the detections at the remote sites and the central station allows for the determination of the meteoroid velocity (Baggaley et al., 1994; Jones et al., 2005; Janches et al., 2015). Given the position, velocity, and observation time of a meteoroid relative to an observer (e.g. a radar antenna), we employ a patched-conics approach (a method to simplify trajectory calculations for spacecraft in a multiple-body environment Wiesel, 1997) to obtain the meteoroid's geocentric and heliocentric orbits. For each of the two orbits, the central body (i.e. the Earth in our case) is assumed to provide the dominant force acting on the meteoroid and is determined by the distance of the meteoroid from the relevant celestial bodies as well as their mass properties. All other forces (e.g. atmospheric drag) are modeled as perturbation forces and are not considered in the estimation of the meteoroid's nominal orbit.

Since SAAMER-OS is not currently using any model for the meteoroids' deceleration in the Earth's atmosphere, we note, that the reported geocentric speed is actually a lower limit. The deceleration in the radar observation might play a significant role for low speed meteors (< 25 km s^{-1}), while for meteors with high geocentric speeds (> 60 km s^{-1}) the deceleration correction is more likely to be negligible (Brown et al., 2004).

Table 1 shows comparisons of 21 showers detected both by SAAMER-OS and CMOR. For each shower we show the solar longitude of the peak λ_{max}, the sun-centered longitude $\lambda - \lambda_0$, the sun-centered latitude β, the geocentric velocity V_g in km s^{-1}, and the geocentric velocity difference Δ_{V_g} measured by SAAMER and CMOR respectively. Note, the value of V_g is presented with the deceleration correction for CMOR while for SAAMER-OS no deceleration correction was applied. We also show a strength of the detection of the shower compared to the compared to background activity σ_{wave} for both SAAMER and CMOR (for more details about σ_{wave} see Section 4). Comparison of common CMOR and SAAMER-OS showers shows similar speeds within uncertainties with the deceleration being a generally second order correction. We note that most of the differences where the shower peaks are observed at the same time show an overall tendency for CMOR's speeds to be slightly higher, as expected given the deceleration correction applied to all

CMOR meteors. Interestingly, when we compare the geocentric velocities of these showers to those resulting from optical observations (Jenniskens et al., 2016b,c,d; Jenniskens and Nénon, 2016) the geocentric velocity of all comparable radar showers is systematically lower for the case of SAAMER-OS results. On average, the measured geocentric velocities by optical systems are 2 km s^{-1} higher. This shows how critical it is to accurately correct the observations for deceleration effects. In addition, since SAAMER-OS observes systematically smaller meteors than both, CMOR and CAMS, the lower geocentric velocities may be due also in part a result of different dynamics of meteoroids streams. While this issue is important, it is currently beyond the scope of this manuscript and will be addressed in later work.

4. Wavelet-based Analysis Methodology

As in B2010, we compile the data into one composite representative year for meteors with complete information about their radiant location and incident velocity. Janches et al. (2015) showed that the average error in the radiant location is close to 1°, and the spread of velocities is 10%, which are values comparable to those in B2010. This allows us to use the same method that B2010 used for CMOR, however here we modify the original method in that work based on more than 5 years of additional experience applying wavelet analysis to meteor radiant distributions.

Following B2010, we use the 3D wavelet transform to search for clusters of meteors that, after successfully passing several tests, are deemed to be shower candidates. Since the spread in radiant and velocity distributions of showers is usually best described as a Gaussian (B2010), we adopt the Mex-

Table 1: Comparison of characteristics of 21 common showers observed by CMOR and SAAMER-OS. See the main text description of presented values.

IAU	$\lambda_{\max}$	$\lambda-\lambda_0$	β	V_g	σ_{wave}	$\lambda_{\max}$	$\lambda-\lambda_0$	β	V_g	σ_{wave}	Δ_{V_g}
	SAAMER-OS					CMOR					
ETA	46	293.7	7.2	64.2	52.2	45	294.2	7.8	63.6	257.4	0.6
OCE	47	330.4	-13.8	36.5	26.8	49	331.0	-13.1	37.0	76.3	-0.5
ARI	79	331.5	7.2	40.5	6.5	81	329.3	7.5	39.1	125.2	1.4
SZC	80	218.9	-13.5	35.9	34.6	80	219.8	-13.3	37.7	45.7	-2.2
NZC	101	210.4	13.5	36.5	19.2	101	210.6	13.6	37.5	44.9	-1.0
MIC	104	208.5	-13.3	35.9	15.1	104	209.8	-12.2	38.0	8.0	-2.1
PAU	125	215.3	-19.5	39.9	17.4	135	213.5	-18.5	44.0	14.8	-4.1
SDA	125	209.5	-7.5	39.9	141.0	126	210.1	-7.6	40.7	177.7	-1.8
CAP	127	178.6	9.7	24.4	16.3	123	179.9	9.0	22.0	24.4	2.4
NDA	136	210.3	7.7	38.1	7.0	139	208.7	7.8	37.3	12.6	0.8
DSX	187	330.8	-11.0	31.4	29.9	186	330.5	-10.9	31.3	89.3	0.1
OLP	199	236.8	-40.8	26.7	11.8	203	236.8	-36.9	25.5	70.0	1.2
ORI	207	248.3	-8.3	64.2	7.6	208	247.3	-8.1	65.4	82.5	-1.2
NOO	248	205.3	-9.0	41.7	9.8	246	204.5	-8.1	43.1	83.2	-1.4
SSE	274	326.6	18.0	42.3	14.5	275	325.4	20.5	42.3	22.2	0.0
DHY	275	230.4	-30.5	49.9	6.9	266	231.5	-28.2	54.5	18.4	-4.6
AHY	284	208.4	-25.8	42.3	13.1	286	207.4	-26.4	43.2	32.8	-0.9
XSA	288	353.1	6.7	25.5	20.9	288	353.9	6.6	25.3	12.8	0.2
DCS	299	0.8	-9.5	23.7	16.3	301	359.2	-9.3	23.8	12.9	-0.1
MHY	303	228.1	-32.3	35.4	12.4	300	224.7	-29.3	39.1	23.8	-3.7
DCS	305	356.4	-8.5	24.4	11.2	301	359.2	-9.3	23.8	12.9	0.6
MHY	310	221.1	-24	36.5	17.0	300	224.7	-29.3	39.1	23.8	-2.6
AAN	312	214.8	-19.5	41.1	19.1	312	215.1	-18.9	43.2	62.3	-2.1

ican hat mother wavelet to produce a Wavelet coefficient, described by Eq. 1, at a given point $(\Lambda_0, \beta_0, V_{g0})$. For our wavelet search we use the following variables: $\Lambda = \lambda - \lambda_0$, where λ is the ecliptic longitude of the geocentric radiant, λ_0 is the solar longitude at the time of occurrence of the meteor, β is the ecliptic latitude, and V_g; the geocentric speed. The advantages of using sun-centered ecliptic coordinates is that it minimizes shower radiant drift and typically restricts the small remaining drift to be parallel to the ecliptic plane, in contrast to the large Earth-motion-induced drifts found when using right ascension and declination. B2010 did not explicitly expand the wavelet search to the fourth dimension, i.e. in time, since it provided no significant improvements compared to the 3D method. Additionally, from a single site on Earth, radiants over the entire sky are only sampled with a cadence of one day (roughly one degree in solar longitude) so shorter intervals have artificial biases. Following the same approach we divide our composite year of data into 360 bins in λ_0, which also provides benefits in lower memory usage and higher parallelization of the wavelet search. For our dataset we apply:

$$
\begin{aligned}
W_c(\Lambda_0, \beta_0, V_{g0}) = & \frac{1}{(2\pi)^{3/2}\sqrt{\sigma_\Lambda \sigma_\beta \sigma_{V_g}}} \int_{V_{g\min}}^{V_{g\max}} \int_{-\infty}^{+\infty} \int_{-\infty}^{+\infty} N(\Lambda, \beta, V_g) \\
& \left(3 - \frac{(\Lambda_0 - \Lambda)^2}{\sigma_\Lambda^2} - \frac{(\beta_0 - \beta)^2}{\sigma_\beta^2} - \frac{(V_{g0} - V_g)^2}{\sigma_{V_g}^2}\right) \times \\
& \exp\left(-0.5\left[\frac{(\Lambda_0 - \Lambda)^2}{\sigma_\Lambda^2} + \frac{(\beta_0 - \beta)^2}{\sigma_\beta^2} + \frac{(V_{g0} - V_g)^2}{\sigma_{V_g}^2}\right]\right) \\
& \mathrm{d}\Lambda \mathrm{d}\beta \mathrm{d}V_g
\end{aligned}
\tag{1}
$$

where σ_Λ is the size of the probe in the ecliptic longitude direction, σ_β is the size of the probe in the ecliptic latitude direction, σ_{V_g} is the size of the velocity probe, and $N(\Lambda, \beta, V_g)$ is the number of meteor radiants at spatial coordinates (Λ, β) with geocentric speed V_g to compute the wavelet coefficient, W_c. It is important to note that this transformation is not unit invariant, thus a change of angular units from degrees to radians will result in different values of wavelet coefficient. However, as we will see later, the number of detected showers is unit invariant. We adopt in our analysis the same unit convention utilized by B2010 (i.e., degrees for angles and km s^{-1} for velocities). Interpretation of the coefficient $N(\Lambda, \beta, V_g)$ from Eq. 1 can be challenging, since it is effectively an array of delta functions ignoring measurement uncertainty; i.e. $N(\Lambda, \beta, V_g)$ is either unity at the exact position of the meteor in (Λ, β, V_g) space or zero everywhere else. In the case of real measurements, however, each radiant is defined with some uncertainty. A better approach would be to represent each radiant as its normalized probability error density function and perform a wavelet search over this uncertainty-smeared space, but at the expense of computational speed. In this case, we might benefit from binning our dataset in the three dimensional space, which will dramatically decrease the computational demands of the wavelet search process since Eq. 1 becomes a discrete sum. Note, the binning should be fine enough to adequately represent the distribution of meteors in the plane of the sky. B2010, however, used the continuous form of Eq. 1, which removes any potential problems with different bin sizes requiring more computational power. In this study we adopt the same settings as used in B2010.

To isolate local temporal maxima in W_c we determine the median value at each sun-centered radiant point throughout all 360 degree bins in solar longitude for the whole year. Thus we find W_c at each point (Λ, β, V_g), determine its yearly median, and discard all points 3σ above the median. This

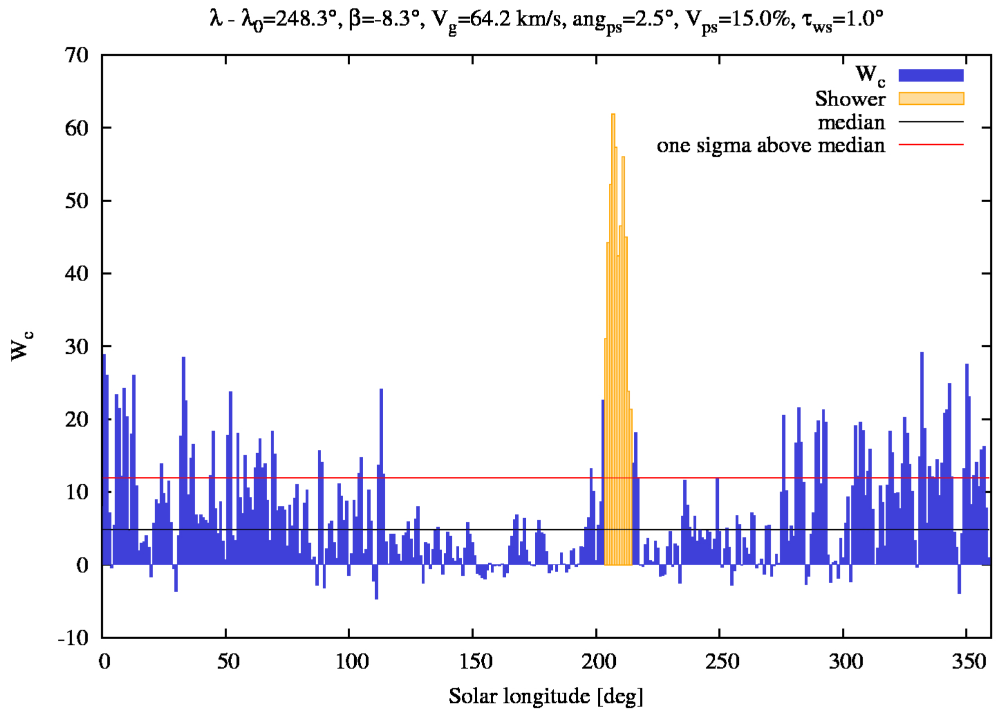

Figure 4: Annual time variation of W_c for the Orionids meteor shower located at $\lambda - \lambda_0 = 248.3°$ $\beta = 8.3°$, with the geocentric speed $V_g = 64.2$ km s^{-1}. The angular probe size in this case is $\sigma_\Lambda = \sigma_\beta = 2.5°$, while the velocity probe size $\sigma_{V_g} = 15.0\%$. The variable $\tau_{\rm ws} = 1.0°$ determines the temporal window selection, which in this case means that we bin data in integer values of the solar longitude.

iterative procedure continues until all values of W_c during the whole year are below the 3σ limit; i.e. we remove potential shower activity during the year (both the shower of interest and other showers which might occur in a similar radiant position) and obtain the wavelet profile of the annual average radiant background at that sun-centered radiant location. An example of the resulting annual time variation of W_c is shown in Fig 4. The annual median is the baseline from which we determine how significant is an excursion in the local W_c found during the wavelet search.The number of standard deviations of this W_c maximum above the median is given by σ_{wave}. Our shower significance level is then stated as the σ_{wave} of the shower maximum. The interpretation of σ_{wave} is straightforward. While W_c might be for some potential showers quite large compared to background, these potential showers might be, in fact, fluctuations of the background and thus should be discarded. On the other hand, using σ_{wave} we can easily detect these artificial showers and remove them from our search. B2010 found that at their peak activity, the most prominent showers had $\sigma_{\text{wave}} > 100$. They further found (empirically) that any shower candidate with a core $\sigma_{\text{wave}} > 3$ might potentially be a shower, though the false positive rate increases significantly once $\sigma_{\text{wave}} < 8$. Additionally, we also require the number of individual radiants used in the calculations of W_c (which is found numerically by counting all radiants outward 3 probe sizes from the radiant of interest) to be more than 30 meteors to avoid false positives in regions with low number statistics (e.g. anti-apex direction).

An additional modification to the B2010 method is to limit the background wavelet coefficient computation throughout the year to periods when the radiant has a zenith angle less than 80°. These W_c are omitted from the annual median computation since the collecting area of such radiants varies significantly throughout the year and we found through experimentation that the resulting small number fluctuations in radiant number tend to produce an artificial contribution to the annual median value, resulting in erroneous σ_{wave} values.

We also must determine the increments for the search steps in (Λ, β, V_g)

space as well as choose angular ($\sigma_\Lambda, \sigma_\beta$) and velocity ($\sigma_{V_g}$) probe sizes. Ideally, we would use infinitesimal steps in (Λ, β, V_g) space, however, the computational complexity increases as the cube of the number of bins in our 3D phase space. For our search we used $0.25°$ steps for angular variables (Λ, β), and 1.5% step in V_g, setting the precision bounds for the resulting shower radiants. The percentage step in V_g is used to capture characteristics of the investigated populations of meteors, in our case we investigate meteors with V_g between 11 and 72 km s^{-1}. The probe size selection is complicated as different showers have distinct angular, velocity, and temporal spreads which result in different sensitivity to selected probe sizes. With potentially three different probe sizes, the time complexity increases proportional to the cube of the number of probes; here we limit the computational time by setting $\sigma_\Lambda = \sigma_\beta$. To identify the optimal probe sizes, we chose the strongest meteor shower observed by SAAMER-OS with well established orbital characteristics (B2010), namely the South δ Aquariids (SDA; $\Lambda = 210.1°, \beta = -7.6°, V_g = 40.7$ km s^{-1}). We then computed $W_{c_{\max}}$ at the time and radiant location of the shower maximum with variable probe sizes both in angular and velocity space. Since the position of $W_{c_{\max}}$ for the SDA in the SAAMER-OS data set might be different from literature values, our search was performed in a region with $205° < \Lambda < 215°$, $-10° < \beta < -5°$, and $36 < V_g < 44$ km s^{-1}. Fig. 5 shows the results of our search for an optimal probe size. From Fig. 5 we see that the best probe size settings are $\sigma_\Lambda = \sigma_\beta = 2.5°$, and $\sigma_{V_g} = 15\%$. These settings were used in all of our subsequent wavelet searches. Having chosen our optimal probe sizes, the next stage in the shower search takes the array of local maxima and links them spatially and temporally. In our search

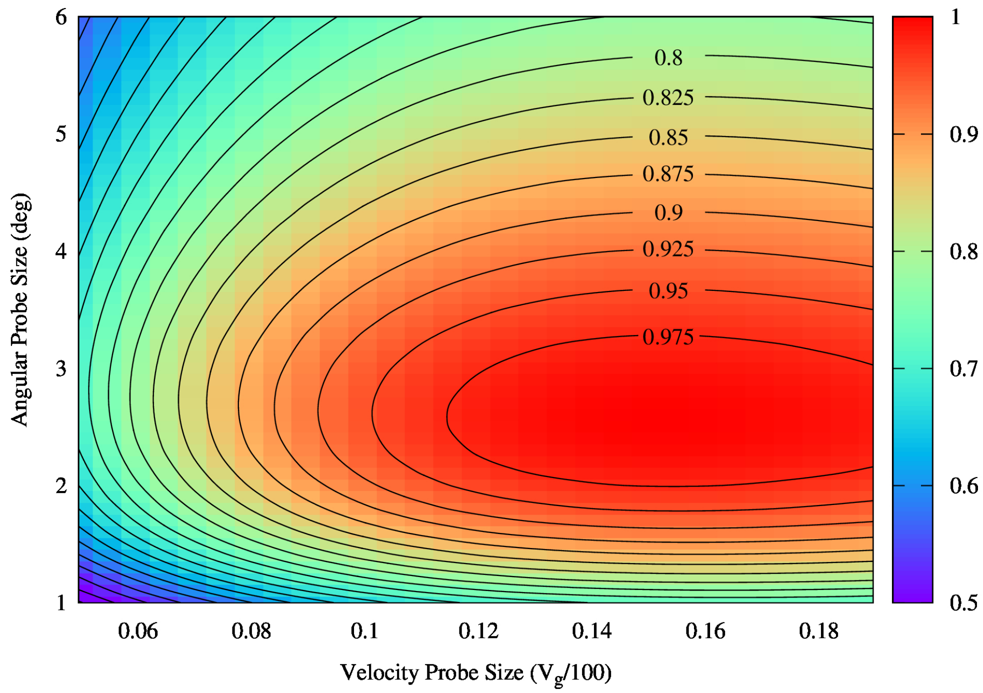

Figure 5: Contour plot showing the wavelet coefficient maxima $W_{c_{\max}}$ on the date of maximum activity at the peak radiant location of the South δ Aquariids meteor shower in velocity and angular probe size phase space. The color coding represents values of $W_{c_{\max}}$ normalized to unity. Here the step in the angular space was 0.1°, and the step in the velocity space was 0.5%.

linkage approach, we expanded the original idea of B2010 and perform our linking procedure in two stages.

In the first stage we considered identified points as part of a single linked stream if the location of the W_c was separated by less than 2° in angular coordinates and less than 10% in geocentric velocity V_g and if the separation in solar longitude was below 2°. This first stage works particularly well for finding stream cores. All linked showers from this first stage analysis, together with their characteristics, wave profiles, and orbital elements can be found in the Supplementary Material[1].

During this first stage, we observed that different linked chains of maxima were associated with the same shower. This is due to the very strict linkage constraints whereby the maximal angular and velocity linkage values are too low. This results in slicing one longer duration shower into several separate chains. To determine if the linked chains are truly separate showers we performed a second more permissive linkage cycle using slightly wider constraints increasing the maximum angular radiant spatial separation to 3° and the maximum difference in V_g to 15%. All linked showers found in the second stage, with their characteristics, σ_{wave} profiles, and orbital elements can also be found in the Supplementary Material.

In total, the first stage of our linking procedure resulted in 133 shower candidates, while the second step using looser criteria provided an additional two candidates for a total of 135 potential showers (see Supplementary Material for more details). From this initial set of potential showers, we applied

[1]See ftp://aquarid.physics.uwo.ca/pub/peter/SAAMER_paper/supplementary.pdf

several further filtering procedures. The reason for these additional filters is simple: we seek only high-quality showers which will be likely confirmed by independent observers in the future. All candidates were required to have a duration of at least 4 days (or 4 degrees in solar longitude). Furthermore, we required that the core (the maximum of the linked chain with the highest value of σ_{wave}) of the candidate must have $\sigma_{\mathrm{wave}} > 6$. Note, that these additional filter conditions were not used in B2010 and would have resulted in the removal of 29 of the 117 identified meteor streams in that earlier work. Of those 29 streams only 5 have been confirmed by other surveys, suggesting that some may be spurious.

5. Results and Analysis

After applying these previously mentioned association techniques and filters, our survey resulted in the identification of 52 meteor streams, 26 of which have not been previously identified according to the IAU Meteor shower list. It is important to note that, although we performed two stages of linking, some streams might actually be part of a larger complex. In this manuscript, we report our findings in two sections: Section 5.1 will describe the showers that are listed in the IAU Meteor Shower Catalogue at the time this work was been conducted, independent of whether they are considered established or not. In Section 5.2 we describe the showers that were not listed in the IAU Meteor Shower Catalogue and thus we consider them as new showers. For more details regarding our shower selection process and the raw results from our shower search the reader can refer to the Supplementary Material accessible online.

5.1. IAU Catalogue Showers

In this Section we describe our results for showers identified by our search method that we can associate with showers listed in the IAU Meteor Shower Catalogue as of February, 2016 (Jopek and Kaňuchová, 2014). We compared the solar longitude, radiant location in sun-centered coordinates, and the geocentric velocity of all IAU MDC showers with those resulting from our search. We consider a positive association when: 1) the value of the solar longitude reported in the IAU list falls within the duration of the shower period during which SAAMER-OS detected it, 2) the radiant location was within 3° of that reported in the IAU list, and 3) the geocentric velocity was within 10% difference. Numerous showers in the IAU list have more than one reported set of parameters. In those cases we treated all reports with equal weight. We considered the IAU MDC showers the same as our detected showers as long as one set from the IAU MDC matched our association criteria. Several showers were associated with more than one reported IAU MDC shower. These cases were treated separately, taking into account whether the IAU MDC lists the reported shower as established and has a well supported set of parameters. Table 2 summarizes the results described in this section where the showers are sorted according to their solar longitude at which highest wavelet coefficient W_c occurs.

In the following paragraphs we provide specific comments about showers listed in Table 2. We will provide comments only for selected showers.

η Aquariids (ETA)

ETA is the second strongest shower observed by SAAMER-OS with a strength over 50σ above the annual median. The timing and radiant position are in good agreement with the IAU database, while our reported geocentric velocity $V_g = 64.2$ km s^{-1} is on the lower end of all reported values being slightly lower than that reported by Brown et al. (2008) and B2010, possibly reflecting deceleration in the SAAMER-OS measurements.

Southern Daytime ω Cetids (OCE)

OCE is a strong shower in our sample with $\sigma_{\rm wave} = 26.8$ lasting for more than 40 days. This gives us strong confidence that the shower is real. OCE is an established shower that has been reported numerous times in the IAU MDC database. The solar longitude of the peak in our search falls between values reported by Brown et al. (2008) and B2010. Different timing of the peak also changes RA and Dec, however the sun-centered coordinates are independent of such a drift. Our reported values are in agreement with Brown et al. (2008) and B2010.

Daytime Arietids (ARI)

ARI is located within the Helion source, and thus it is a daytime shower, observations of which are almost exclusive to radars. SAAMER-OS observation of this shower places the maximum later than other reported values (B2010, Jenniskens et al., 2016b), however the position and the geocentric velocity are almost identical to the values reported by B2010. While the activity of this shower is quite weak as seen by SAAMER-OS (just barely above our minimum 6σ threshold due to the high northern declination of the radiant) at the time of maximum we determined the semimajor axis $a = 2.48$ au, which is a higher value than previously reported by other radars (Bruzzone et al., 2015) but closer to optical observations (Jenniskens et al., 2016b).

Days on either side of the peak, however, are comparable to the speeds and mean orbits reported in Bruzzone et al. (2015).

Southern June Aquilids (SZC)

SZC is the third strongest shower in the SAAMER-OS sample. This established shower has less than 150 reported meteors according to the IAU database; this number increases up to 500 when we include results of B2010. SAAMER has measured SZC meteors with position and timing almost identical to B2010. The geocentric velocity of SZC from SAAMER-OS observations is approximately 10% lower than previously reported. We note that Jenniskens et al. (2016b) reports the shower peak at the solar longitude $\lambda = 104°$ which disagrees with our findings and with those of B2010. One potential source explanation is that Jenniskens et al. (2016b) mistakenly exchanged SZC for MIC (Microscopiids), which has similar radiant/speed values.

Southern May Ophiuchids (SOP)

SOP is not currently an established IAU MDC shower having only a handful of reported meteors since it is not easily observable from the Northern hemisphere, where most of the surveys to date have taken place. SAAMER-OS, however, detected SOP as a stronger shower with $\sigma_{\text{wave}} = 15$, duration of 33° in the solar longitude, and positive drift in both RA and Dec. The peak of SOP ($\lambda = 81°$) appears later than previously reported ($\lambda = 65.2°$ Jopek et al., 2010), however, the orbital elements for this shower are similar to those determined by Jopek et al. (2010).

Northern June Aquilids (NZC)

NZC is a shower of medium strength lasting for more than 30 days from SAAMER measurements. This shower is not considered established in the IAU meteor database despite many reports with significant numbers of meteors (B2010, Jenniskens et al., 2016b). The characteristics of the NZC in our survey agree with previously reported values with one exception in the geocentric velocity $V_g = 36.5$ km s^{-1}, where our value is 5% smaller, possibly due to lack of deceleration correction.

Microscopiids (MIC)

MIC is one of the stronger showers in the southern hemisphere, and was previously reported only by B2010. There is a possibility also that this shower may have been misidentified by Jenniskens et al. (2016b) as SZC. Our reported timing, radiant location are almost identical to those reported by B2010, while our geocentric velocity is approximately 6% smaller.

Piscis Austrinids (PAU)

PAU is another strong shower in the southern hemisphere, that is difficult to observe by facilities in the northern hemisphere. This shower is considered established by IAU despite having less than 200 reported meteors. Interestingly, the timing of the peak of PAU is 10° earlier and the speed 10% smaller than the value reported by B2010. However, the radiant location is almost identical. The activity is broad and the peak not well defined so this difference may reflect the broadness of the shower profile. The velocity difference is also the reason why the reported orbital elements are different to those we found in this work.

South δ Aquariids (SDA)

SDA is the strongest ($\sigma_{\text{wave}} = 141$) and the longest lasting (more than 50 days) shower in our sample. This shower is well established. The characteristics we determined and report here agree well with published values, though our geocentric velocity $V_g = 39.9$ km s^{-1} falls into the slower end of reported values, again possibly due to the fact that we are not correcting for deceleration.

October Leporids (OLP)

OLP is a stronger shower in the southern hemisphere previously reported only by B2010. Due to its far southern radiant location, B2010 did not see as many meteors as for other showers, however, its significance level in CMOR data of $\sigma_{\text{wave}} = 70$ makes this shower one of the strongest southern hemisphere showers observed by CMOR. Our results are in good agreement with those reported by B2010. An outstanding feature of this shower from both CMOR and SAAMER measurements is its high inclination, Aten-like orbit and its unknown parent body.

β Canis Majorids (MCB)

MCB is a weak shower lasting for only 5 days in SAAMER data. It was previously reported by Andreić et al. (2014) with only 20 meteors. Our reported values agree well with Andreić et al. (2014) however, due to the low significance level with $\sigma_{\text{wave}} = 7$, the activity profile is not completely convincing (see the Supplementary Material) and it is unclear whether this is a real shower or just a fluctuation in the background.

November Orionids (NOO)

NOO is an established shower in the southern hemisphere that has been widely reported according to the IAU MDC. SAAMER detects NOO as a weaker shower ($\sigma_{\mathrm{wave}} = 9.8$) with characteristics very similar to reported values. Interestingly, NOO is very strong when observed by optical systems Jenniskens et al. (2016b). While the parent body for NOO remains unknown, its orbital elements suggest a cometary origin. Even though our measured geocentric velocity is slightly lower than previously reported values, and thus so is the semimajor axis $a = 4.68$ au, we confirm its probable Halley-type comet (HTC) or Oort Cloud comet (OCC) origin.

e Velids (EVE) / Puppid-Velid I Complex (PUV) / b Puppids (PVE)

Our search resulted in provisional detection of a shower that can be associated with three non established IAU MDC showers, namely the EVE, PUV, PVE. Since the timing, radiant location and the geocentric velocity are only available for EVE (Jenniskens et al., 2016b), we identify our results with this shower. This shower is located at a high southern hemisphere latitude, presumably the main reason it remained unknown until 2016. In comparison with Jenniskens et al. (2016b) our shower has an earlier peak activity occurring at $\lambda = 250°$, slightly different radiant location, and a lower geocentric velocity $V_g = 39.9$ km s^{-1}. However, this shower is one of the strongest in our dataset with $\sigma_{\mathrm{wave}} = 13.6$. It is active for a period of 21 days, and is peculiar because of its very highly inclined orbit $I = 71.9°$, typical for the South Toroidal source region.

December Hydrids (DHY)

DHY is the second weakest shower in Table 2 even though its observing geometry is good for SAAMER. This shower was exclusively reported by B2010 with more than 600 meteors and very good significance level, but has not yet been categorized as established. The timing and radiant location are in good agreement with B2010, while our reported speed is 10% lower. However, we must again remain cautious in this case, since our search method resulted in a rather weak activity. The shower duration from SAAMER-OS observations is 5 days, which is shorter than reported by B2010 (20 days).

Daytime Capricornids-Sagittariids (DCS)

DCS is a minor not established shower in the southern hemisphere that was repeatedly reported in the 70's by Sekanina (1973, 1976) and then rediscovered 30 years later by B2010. Although the timing, radiant location, and geocentric speed determined from our survey are different from earlier reports, it is in a good agreement with B2010. The shower is listed twice in Table 2 since our search code interpreted this shower as two separate showers with very similar, though spatially separated enough, radiant locations and geocentric velocities. However, their durations do not overlap, with an approximate 3 day gap.

μ Hydrids (MHY)

MHY is a shower first reported by B2010. It is a southern hemisphere shower not yet established by the IAU MDC ($\beta = -32.3°$). MHY is one of the weaker showers in SAAMER-OS survey ($\sigma_{\mathrm{wave}} = 12.4$) with slightly different timing of the peak, radiant location and geocentric velocity than those reported by B2010. Since the shower is located significantly below the ecliptic plane, the observation geometry of B2010 might play a significant role in CMOR's ability to observe it, and thus the exact position may need to be refined. Interestingly, our searching code detected another shower with similar peak timing, radiant location, and geocentric speed, that was actually much stronger than the shower reported by B2010. We also associated this shower with MHY (the second record in Table 2). The radiant separation of these showers is quite significant, and it would be very rare that two different showers appear at the same time in a very similar place with comparable geocentric velocities. Nevertheless, we are confident that this shower is real and supporting the findings of B2010, who reported a very peculiar orbit ($a = 1.08$ au, $e = 0.77$, and $I = 71.8°$). Such orbits are unique in the Solar System given the fact that currently there is no known body with similar orbital elements.

5.2. New Showers

In this section we describe new showers that, to the best of our knowledge, are not associated with any shower listed in the IAU Meteor Shower list at the time of this investigation. The results are listed in Table 3.

30 Ophiuchids (THO)

THO is a weaker north apex meteor stream lasting for 5 days, which appears to have been undetected in north-hemisphere surveys. Its significance level ($\sigma_{\text{wave}} = 6.5$) is very near the limit of our linking criteria, and thus more data is required to confirm this shower candidate as an established shower. THP has a retrograde ($I = 138.1°$) and eccentric orbit ($e = 0.615$), which suggests cometary origin, probably from a Halley-type comet.

Octantids (OCD)

OCD is a new stronger shower ($\sigma_{\text{wave}} = 10.8$) with a very high southern ecliptic latitude. This shower lasts for 20 days and is one of the prominent showers of the southern toroidal sporadic source. Its very distinctive Aten-like orbital elements ($a = 0.96$ au, $e = 0.174, I = 65.1°$) and duration suggest that OCD is a product of cometary activity of a Halley-type comet, that has been evolving for several thousand years.

ρ Phoenicids (RPH)

As the third strongest new shower ($\sigma_{\text{wave}} = 20.9$), RPH is highly visible in our dataset even without the use of any complex processing techniques. This shower lasts for 10 days and is part of the south toroidal source being again most probably associated with one of the Halley-type comets due to its peculiar highly-inclined orbit.

o Pavonids (OPA)

OPA is a weak shower located in the south toroidal region lasting for 5 days. It has an orbit with a very high Tisserand's parameter with respect to Jupiter ($T_{\text{J}} = 6.3$), Aten-like orbit, and very high inclination. This shower is very peculiar, potentially originating from the population of Near-Earth Asteroids (NEAs) or highly evolved from an HTC-parent.

υ Pavonids (UPA)

At first this shower appeared to be a continuation of OPA, however, a large gap between these two showers and a noticeably different radiant location led us to consider these to be different showers. Accordingly, the resulting σ_{wave} makes this shower the weakest in this survey, and thus more observations are required to determine whether this shower is real or just a fluctuation of the background. Having very similar properties to OPA this shower is also a candidate for either a NEA origin or highly evolved HTC.

Telescopiids (TEL)

TEL is a shower at the bottom edge of the anti-helion source lasting for 10 days. Although the significance level ($\sigma_{\text{wave}} = 6.4$) is low, this shower has a very distinctive activity profile (see Supplementary Material) giving us confidence that this shower is indeed real.

α Sagittariids (ASG)

ASG is one of showers that are at the very limit of our acceptance criteria with a very short duration of 5 days and limiting significance level $\sigma_{\text{wave}} = 6.2$. Nevertheless, if real, this anti-helion shower might be one of the showers caused by Jupiter Family comets due to its favorable inclination and highly eccentric orbit.

β Aquilids (BAD)

BAD is one of the few new showers in the northern hemisphere, more precisely in the northern part of the anti-helion source. The fact that this shower has not been observed by northern hemisphere radar surveys raises question about its validity. Lasting for 8 days, this shower is another candidate for a possible NEA origin.

α Phoenicids (APH)

Another from the group of new south toroidal showers, APH is a weaker shower lasting for 6 days that is very peculiar for its orbit with the semimajor axis (a = 0.7 au) lower than Venus. Though this part of the sky is not significantly populated by meteors in the SAAMER-OS sample, the activity of this shower stands out, which gives us considerable confidence that this shower is real.

ζ Phoenicids (ZPH)

ZPH is one of the stronger showers detected by our survey in the south toroidal source ($\sigma_{\text{wave}} = 13.1$). ZPH lasts for 13 days, has a highly-inclined orbit ($I = 76.9°$) and $T_{\text{J}} = 2$, with high e suggestive of a cometary origin, the most probable being from a Halley-type comet.

ψ Phoenicids (PPH)

PPH is the strongest new shower ($\sigma_{\text{wave}} = 26.2$) discovered in the SAAMER-OS dataset by our searching method. Lasting for 23 days PPH is one of the most prominent showers in July observable from the southern hemisphere. With its location in the south toroidal source resulting in its intrinsically highly-inclined orbit ($I = 74.8°$), this shower most probably originates from one of the Halley-type comets. Though its small semi-major axis and modest eccentricity produces $T_{\text{J}} = 4.4$ suggestive of an asteroidal origin, the duration of PPH and its high inclination is clearly the result of long dynamical evolution, with Poynting-Robertson drag perhaps producing the small a, e combination.

λ Caelumids (LCA)

After a period of almost three months in which showers were not detected by SAAMER in the south toroidal sporadic source, LCA was observed in October. LCA is a weaker shower lasting only 4 days - it is very close to the detection limit set by our search criteria. Its orbit is typical of showers found in the toroidal source with very high inclination and the semimajor axis placing its aphelion just below the orbit of Jupiter.

σ Columbids (SCO)

SCO is a shower in the south toroidal source that lasts for 6 days. Since its sun-centered coordinates and geocentric velocity are very similar to PPH, the strongest shower in the south toroidal source, the significance level for this shower is quite low ($\sigma_{\rm wave} = 7.9$). The potential linkage between SCO and PPH will be discussed in the next Section,

γ Sextantids (GSE)

GSE belongs to the southern part of the helion source. Its duration (4 days) and significance level ($\sigma_{\rm wave} = 6.2$) is at the limit of our searching criteria. GSE has an Aten-type orbit with an extreme value of the Tisserand parameter ($T_{\rm J} = 7.4$).

Puppids-Pyxidids Complex (PPC)

This complex consists of 8 showers (THP, ECM, OBP, OAP, OPU, OLV, NPU, NLV) that, utilizing a looser linking criteria, forms a south toroidal shower that lasts for more than 40 days. It is the southern counterpart of the Coronae Borealid complex first reported in the North Toroidal source by CMOR in B2010. All showers have very similar orbits with semimajor axes close to 1 au, low eccentricities, and very high inclinations ($I \sim 67°$). We consider NPU as the core of this complex due to its significance level $\sigma_{\text{wave}} = 9.6$. This complex is similar to NID/QUA/TCB complex (B2010) that is observed in the north toroidal source with one exception - a much lower geocentric velocity. South toroidal showers in this complex are systematically 8-10 km s^{-1} slower, which is more than expected for a deceleration correction alone and makes any genetic association with its north hemisphere counterpart difficult.

ζ Antliids (ZAN)

ZAN is a weaker shower at the edge of the south toroidal source that might be also associated with PPC. However, its location in the sky, shower profile, and higher eccentricity lead us to exclude this shower from PPC.

ιArids (IAD)

This shower is located near the far edge of the helion source. Its activity lasts 5 days and it is characterized by a very eccentric orbit ($e = 0.86$), and low inclination ($I = 14.5°$). This shower is, most likely, a product of a Jupiter-family comet.

ι Lupids (ILU)

ILU is also a shower located within the helion source, even though its position is very close to the south apex source. Its activity lasts for 6 days with the significance level comfortably above the limits ($\sigma_{\text{wave}} = 9.3$). ILU has very similar orbital elements to MHY $a = 1.05$ au, $e = 0.744, I = 66.2°$, and also NHR introduced later in the text. Without further modeling it is difficult to determine whether these showers have the same parent body. Also a very high inclination suggests that this shower may have its counterparts located in, either the North or South Toroidal source.

κ Velids (KVE)

KVE is the second strongest shower in our survey occurring in the south toroidal source and lasting for more than 15 days. KVE is almost identical to the α Puppids reported by Younger et al. (2009). Because the authors did not reported their findings to the IAU working list, we excluded their listing from our association code. Our findings suggest that this stream is one of the streams evolved from Halley-type comets (Pokorný et al., 2014) and may be linked to the complex of showers associated with 96P/Machholz (Babadzhanov and Obrubov, 1992).

θ Carinids (TCD)

TCD is a strong shower within the south toroidal source region lasting for 7 days. Its significance level ($\sigma_{\text{wave}} = 9.8$) is not particularly high because it shares the radiant location, and geocentric velocity with the stronger and long lasting shower EVE. Similar to EVE and other southern toroidal showers TCD is characteristic for its high inclination ($I = 74.5°$) and $T_{\text{J}} < 3$.

6 Puppids (SXP)

SXP is a minor shower in the southern part of the anti-helion source. SXP is quite a short shower lasting for 5 days. The orbital characteristics of this shower are quite peculiar for a shower originating from the anti-helion source, believed to be mainly populated by Jupiter-family comets (Nesvorný et al., 2011). The high inclination of the SXP meteors ($I = 58.6°$) suggests that this shower is more likely a product of a Halley-type comet.

Volantids (VOL)

VOL is one of the strongest showers with a duration of 10 days impacting the Earth almost from the south pole ($\beta = -72.7°$). With a geocentric speed almost identical to the Earth's orbital speed($V_\mathrm{g} = 29.6$ km s^{-1}), this shower clearly exhibits a cometary origin, with a high inclination ($I = 49.1°$) which suggests a Halley-type comet as possible parent bodies. This shower was also recently independently discovered by Jenniskens et al. (2016a).

9 Herculids (NHR)

NHR is a very peculiar shower in this survey since its radiant location is well within the northern hemisphere and thus, it should have been observed by previous surveys. Because of this we cannot discount the possibility that this shower may be the result of an artifact of our searching methodology. NHR is located between the north apex and the helion sources. It has an orbit with high eccentricity and inclination ($e = 0.826, I = 65.5°$), while its semimajor axis is very close to unity. To determine whether this shower is real, or if it was a strong outburst, a longer survey with uniform data coverage is required. As mentioned before, this meteor shower has very similar orbital elements to MHY and ILU.

January μ Velids (JMV)

JMV is a stronger ($\sigma_\mathrm{wave} = 9.8$), long lasting shower (15 days) in the south toroidal source. With one of the highest values of the Tisserand parameter ($T_\mathrm{J} = 6.1$), JMV appears to be another promising candidate for a high-inclination NEO parent or an evolved shower from an HTC source.

ψ Velids (PVL)

PVL is one of the stronger showers in the south toroidal source lasting for 21 days. PVL has almost exactly the same radiant location, and identical geocentric velocity as ZPH, however, their peak activity differs in solar longitude by $\sim 180°$. This suggests that these showers are actually twin showers and thus a product of the same parent body, most probably a Halley-type comet.

ι Antliids (IAN)

IAN is a weaker shower at the southern edge of the anti-helion source that lasts for 6 days. Although its significance level is not high, both the consistent rise and fall of the activity level about the maximum date and its orbital characteristics provide confidence that it is a real shower. Its Aten-type highly inclined orbit suggests a possible NEO origin.

March β Equuleids (MBE)

MBE is a weaker helion-source shower that lasts for 9 days. Its significance level $\sigma_{\text{wave}} = 6.3$ is decreased by the presence of the SSE, which is active for 22 days approximately 3 months earlier and has very similar radiant position in the sun-centered coordinates and similar geocentric velocity. MBE is certainly of cometary origin, having a highly eccentric ($e = 0.965$), and a highly inclined ($I = 68.8°$) orbit.

5.3. Newly identified Meteor Showers - population characteristics

Here we focus on a more global overview of the common characteristics of the new showers identified during the SAAMER-OS survey. The radiant location of the new showers is shown in sun-centered coordinates in Figs. 6

and 7. In these figures the radiant locations are color coded according to the solar longitude where the maximum activity occurred for the IAU list meteor showers (Fig. 6) and for the newly discovered showers (Fig. 7). In comparing these figures, it can be seen that the new showers exhibit a half ring-like structure located about 55° away south of the apex direction. This result is very similar to the northern hemisphere ring identified during the CMOR survey reported by B2010. Showers having radiants within this structure occur during a broad range of solar longitudes, implying that different parent bodies are required to create the observed features. The northern part of this ring is also known for its distinctive distribution of sporadic radiants first reported as a ring-like structure by Campbell-Brown (2008). This sporadic population is believed to be caused by dust released by Halley-type comets (Pokorný et al., 2014). A dynamical model that would reproduce all the observed features along with the temporal variations has yet to be developed.

Figures 8 and 9 are color coded according to each shower's geocentric velocities. The survey resulted in only three showers, two known (ETA, ORI) and one new (THO), with very high geocentric velocities ($v_g > 60$ km s^{-1}). This is less than expected if we compare our results with those from B2010 who found 10 showers at high geocentric velocities. Since, in principle, both radars should be able to detect very fast meteors, this result suggests that either the south apex source is poorer in meteor showers, or an unknown bias at higher geocentric speeds is present in the SAAMER-OS sample.

An interesting result is found when we combine our search results with those from B2010. The ring structure is almost exclusively populated by showers with geocentric velocities in the $35 - 40$ km s^{-1} range. The conser-

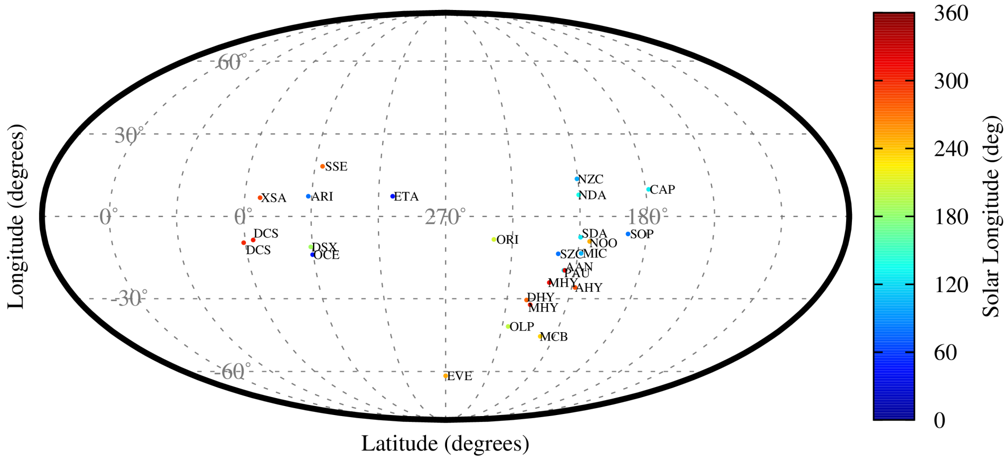

Figure 6: Radiant locations for previously listed meteor showers (IAU) in sun-centered coordinates. The circles are color coded with respect to the shower peak solar longitude and are labeled with IAU 3-letter designations.

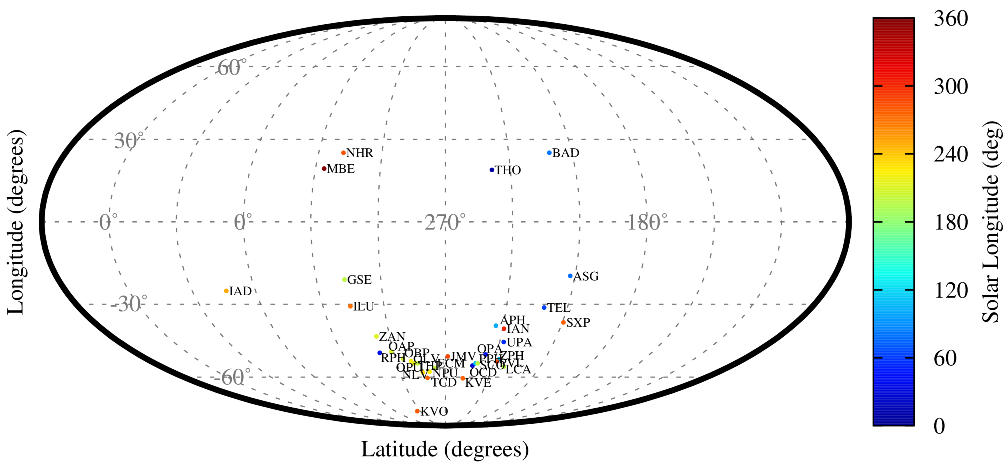

Figure 7: The same as Fig. 6 but for the newly discovered showers in our survey.

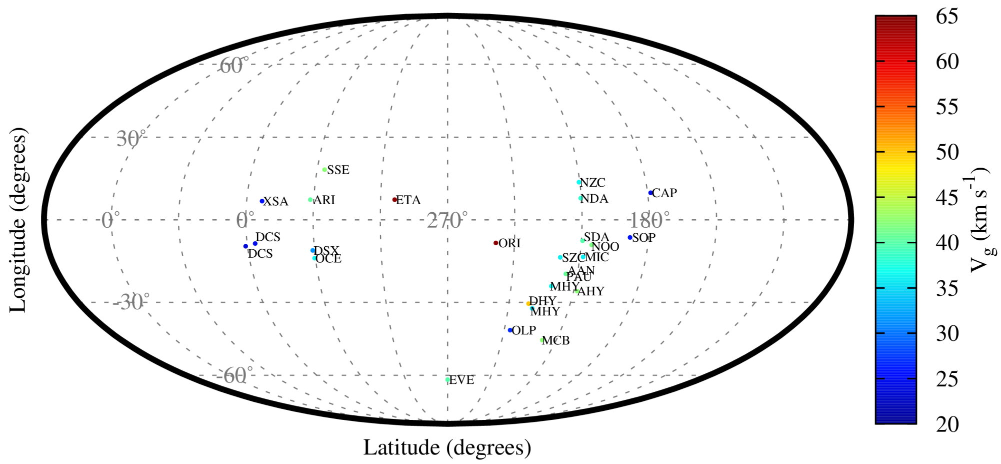

Figure 8: Radiant locations for previously listed meteor showers (IAU) in sun-centered coordinates. The circles are color coded with respect to the geocentric velocity and are labeled with their IAU 3-letter designations.

vation of geocentric speed on the ring results from the Kozai-Lidov mechanics and the preservation of integrals of motion that are an invariant correlated with the angular position on the ring relative to the apex (Pokorný et al., 2014, Sec. 4.3). The helion/antihelion sources are populated by showers with very low speeds around $20-25$ km s^{-1}, in agreement with models of Jupiter-family comets (e.g. Nesvorný et al., 2011), which are believed to be the progenitors of the majority of the meteoroids from these showers. Our survey has not found any meteor shower with geocentric speeds below 20 km s^{-1}, which is somewhat similar to the results reported by B2010 who found only 2 showers close to this limit. This reflects the dramatic decrease in the ionization efficiency at low speeds (Jones, 1997), which results in a factor of 10 decrease in sensitivity for equivalent mass meteoroids with entry speeds of 14

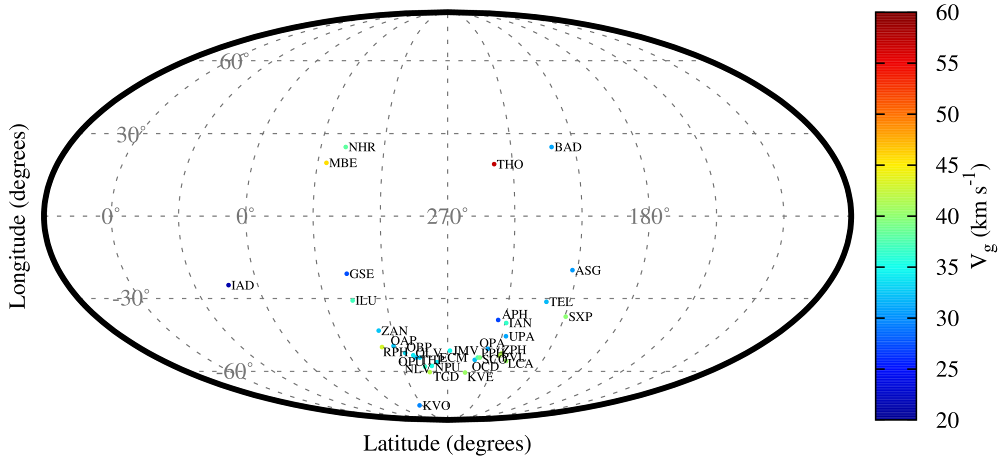

Figure 9: The same as in Fig. 8 but for newly discovered showers.

km s^{-1} compared to 20 km s^{-1}. Figure 10 shows the orbital eccentricity distribution vs. the semimajor axis of detected showers from our survey color coded by their Tisserand parameter with respect to Jupiter. Most of the newly discovered showers (triangles in Fig. 10) have semimajor axes close to 1 and low eccentricities. This combination of orbital elements directly influences the distribution of T_{J} producing the very high values $T_{\mathrm{J}} > 4$ for many of the SAAMER showers. No showers with the semimajor axis larger than 5 au were reported, and only two new showers have the semimajor axis larger than 3 au.

Figure 11 displays the distribution of inclinations with respect to the semimajor axis, showing that most of the new showers cluster at $a = 1$ au and $I \sim 65°$, formed mostly by the showers within the south toroidal source region. There were no new showers discovered below $I < 30°$. This is somewhat expected since this region has been covered by many different

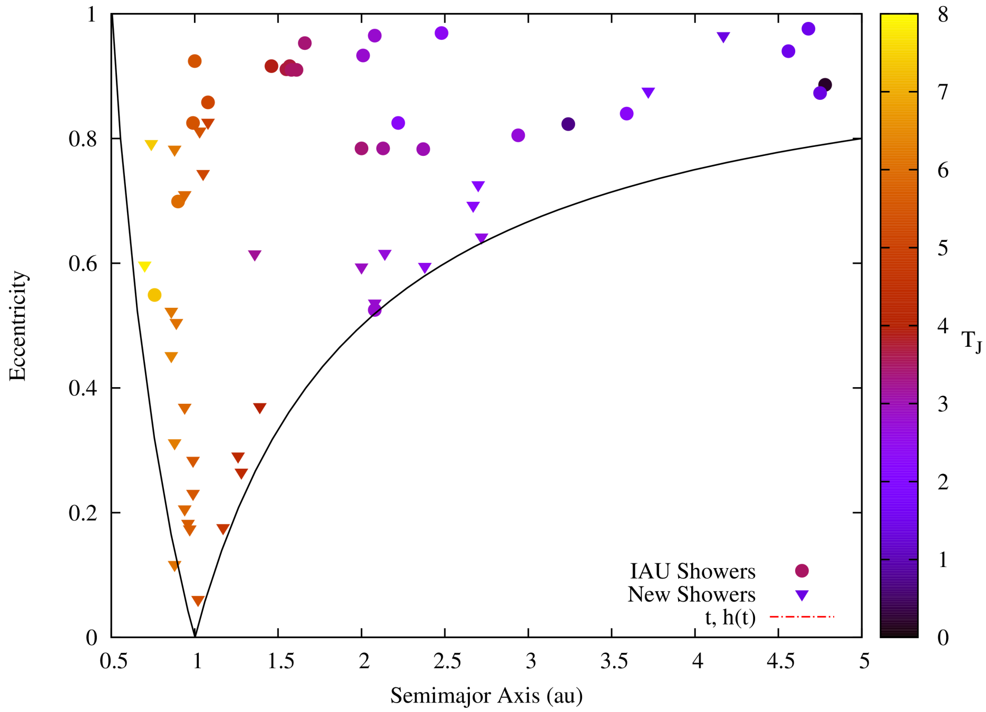

Figure 10: Distribution of eccentricities with respect to semimajor axes of all meteor showers found by our survey. The symbols in this figure are color coded by their Tisserand parameter T_J . Black solid lines denote the region of (a, e) phase-space inside of which impacts on the Earth are possible. The lines denote (a, e) combinations for orbits with perihelion (right hand line) and aphelion distance (left hand line) equal to the Earth's orbit. Newly discovered showers are represented by triangles, while previously known showers by filled circles.

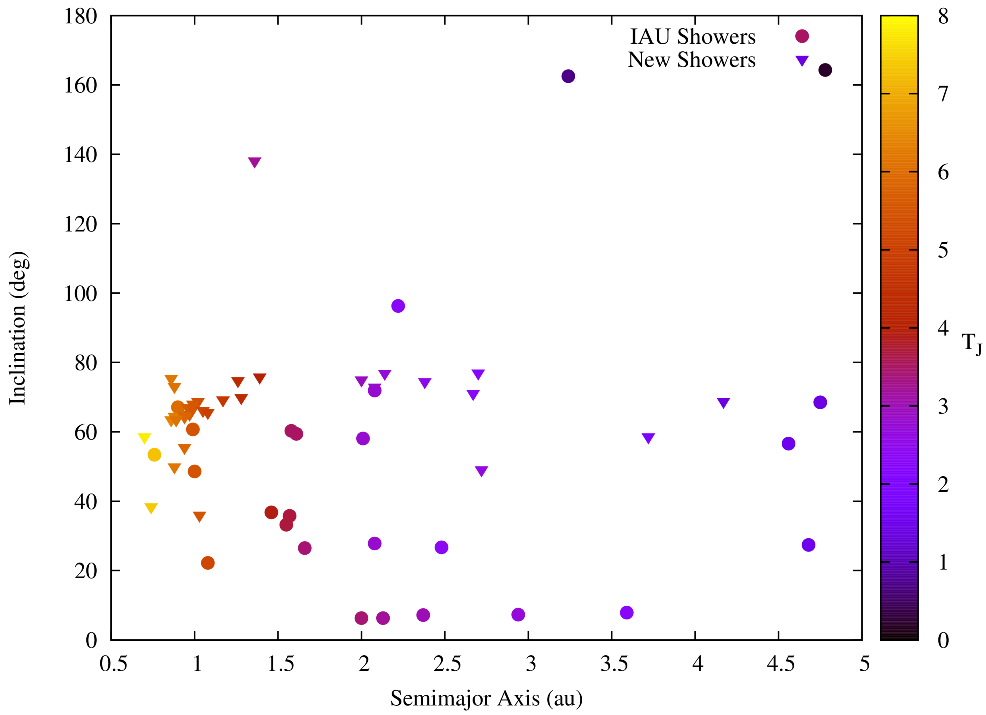

Figure 11: Distribution of inclinations with respect to semimajor axes of all meteor showers found in our survey. As for Figure 10, the symbols are color coded by their Tisserand parameter T_J. Newly discovered showers are represented by triangles, previously known showers by filled circles.

surveys (e.g. B2010 Jenniskens et al., 2016b). Interestingly, only one new retrograde meteor shower was found (THO). It is interesting to note the large number of such high - I, small-e, a showers which mirrors a similar population first reported by CMOR in B2010 for which no immediate parent body population is known.

Figure 12 shows the distribution of inclinations of all showers resulting from this survey with respect to their eccentricity. The majority of SAAMER-OS showers, even those with rather high eccentricities ($e < 0.7$), have inclinations which exceed the Kozai angle ($I \approx 39.2°$) and thus are affected by Kozai oscillations. This may reflect an observational selection effect as showers affected by the Kozai oscillation will typically have much longer dynamical coherence and collisional lifetimes compared to lower inclination streams. Thus we may be able to see backward in time to much older streams in the toroidal sources as a result. In this view, the low-a and e of these streams are simply the result of the Poynting-Robertson circularization of the orbits, having removed the orbits from their original HTC parent orbits, but with the streams remaining in the Kozai due to their high inclination.

5.4. Potential parent body candidates: shower branches, twins and stream complexes

Knowledge of a shower parent body enables modeling of the meteor shower activity through time and allows the connection of properties of shower meteoroids (chemistry, strength, etc.) with a specific object. There is no robust method that enables unequivocal identification of the parent body of all meteor showers. Radiative forces acting on small meteoroids in the mass range observable by radar systems Burns et al. (1979) should lead to a mass dependent segregation in meteoroid orbits relative to the orbit of the parent body over time. This change in orbit size, together with planetary perturbations will produce a meteor shower having a duration directly dependant on its age of ejection from the parent. From Tables 2 and 3, we know that the duration of the meteor showers we measure in our survey range from several to as much as 50 days (as is the case of SDA). For example, the Orionid meteoroid stream (ORI), which lasts for 11 days, is believed to be

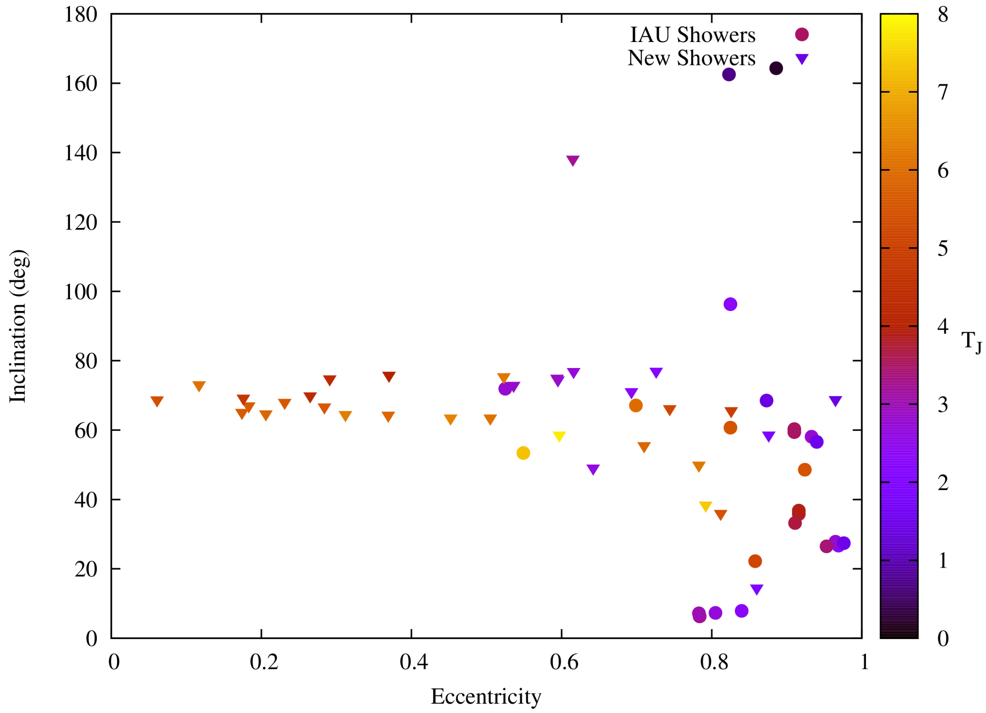

Figure 12: Distribution of inclinations as a function of eccentricites of all meteor showers found in our survey. Symbols are color coded by their Tisserand parameter T_J. Newly discovered showers are represented by triangles, previously known showers by filled circles.

2 500 to 62 000 years old, with the most probable age being 23 000 years (Jones et al., 1989). However, while the shower duration provides a powerful constraint on stream age, such detailed study and modeling of particular meteor showers is beyond the scope of this work.

For this work we use a simpler, but effective approach that considers the orbital dis-similarity criterion developed by Valsecchi et al. (1999). This method uses quantities directly observable by Earth-bound instruments, i.e. the geocentric speed, the right ascension, the declination of the radiant and the solar longitude of the peak of the meteor showers. The applicability of this approach to long lasting showers is more uncertain. However, for many meteor showers this method helps narrow the number of candidate parent bodies efficiently enough to highlight the most possible candidates from a myriad of possible parent objects.

In this work, we calculate D_N, the orbital dis-similarity criterion (Valsecchi et al., 1999), for all showers found in our survey with respect to all objects in the Minor Planet Center Orbit Database[2]. Since the number of potential parent bodies is extremely large, we focus on the three most promising candidates, i.e. objects with the lowest D_N, since showing only the very best candidate on the basis of orbit alone is misleading due to different object sizes. We expect, a priori, that larger parent bodies and comets are more likely to have spawned meteoroid streams now visible at the Earth, everything else being equal. Additionally, we searched for the comet or the object with the lowest absolute magnitude with $D_N < 1$, choosing all comets as

[2] http://www.minorplanetcenter.net/iau/MPCORB.html

more probable parents over Near Earth Asteroids (NEAs) in the final tabulation. Results of our search are shown in Tables 4 and 5.

Examination of Tables 4 shows that the method, while simple, is limited in its utility when applied to more evolved stream-parent body linkages. For example, for the ETAs the known parent body is 1P/Halley (Babadzhanov, 1987), which agrees with what our method produces. In contrast, 1P/Halley is also known to be the parent body for the ORI, which our method did not capture. Thus the results reported in this section must be treated with caution, the main purpose being to provide a series of potential parent bodies which require follow-up simulations to confirm or refute. Through the rest of this section we will focus on the few most promising parent bodies and their possible showers based on this analysis. Since the physical size of these parent bodies is mostly unknown we use a simple relation (Chesley et al., 2002)

$$D = \frac{1329}{\sqrt{p}} 10^{-0.2H} \tag{2}$$

to convert the absolute magnitude H to the body diameter D assuming the albedo p is known (hereafter we use a typical albedo $p = 0.15$ for all parent bodies in this paper).

2003 UL9 is one of the smaller NEO's with an absolute magnitude of 22.5, which translates to an approximate radius of 50 m. Its size is probably too small to be a shower parent body. However, it might be the product of a recent breakup of a larger parent that lead to the formation of the Puppids-Pixidids Complex (PPC).

2009 VQ25, an Apollo asteroid, is also related to PPC according to the orbital dis-similarity criterion, however the similarity with the shower complex is smaller than for the case of 2003 UL9. On the other hand, it's size is approximately 5 times larger than 2003 UL9.

2007 HX4, another NEO with an absolute magnitude of 17.7 (1 km diameter), is another body related to PPC, mostly to its later part being a potential parent body for OPU, OLV, NPU, and NLV.

(2102) Tantalus, based on the latest observations, is a probable binary (Warner, 2015), and has been previously suspected to be a parent body of known meteor streams (Kostolansky, 1998). Its absolute magnitude 16.0 (2-4 km in diameter) and uncommon Q spectral type (Bus and Binzel, 2002) make it an attractive candidate for several newly discovered meteor showers (KVE, TCD, VOL, PLV). Alternatively, this may be part of the broader 96P/Machholz complex of bodies/showers.

2010 BG2 is an asteroid on a peculiar orbit. Although small in size ($H = 19.9$), its comet-like orbit and higher inclination ($I = 42.9°$) may lead to the discovery of a possible progenitor. Its orbit similarity to previously established meteor showers AHY, MHY, and AAN is a promising result.

2009 FG1 is another asteroid from a growing suite of NEOs. With its highly inclined orbit ($I = 69.8°$) it is a potential parent body for four newly discovered showers (LCA, SCO, THP, ECM). However, since its size is rather small ($H = 18.8$) it's unlikely that this particular body is the real parent body of all mentioned showers, but may be genetically related as a sibling from an earlier breakup.

C/2015 P3 (Swan) is a new comet discovered in Australia, reported by Mattiazzo et al. (2015). Due to its high inclination $I = 58.2°$, C/2015 P3 (Swan) is a promising candidate for many newly discovered showers. However, its orbital period of more than 3500 years makes further observations quite challenging.

C/2013 R1 (Lovejoy) is very similar to C/2015 P3 (Swan). Its inclination is very promising as a candidate for north/south toroidal showers, however the orbital period of this comet is even longer, more than 6000 years (Wirström et al., 2016).

P/2010 H3 (SOHO) is another designation for P/2004 V9 or P/1999 J6 and is believed to be a parent body of ARI (Jenniskens et al., 2012), although recent modeling of meteor streams suggests that these objects alone cannot explain the ARI activity profile (Abedin et al., 2017). Our method indeed shows a reasonable linking between this comet and ARI, however, more streams like SZC or newly discovered ASG show a very good match, consistent with broader identification with the 96P Machholz group (Jenniskens, 2006).

C/1995 O1 (Hale-Bopp), one of the brightest comets recently observed at Earth, is a very promising candidate for four newly discovered showers, namely KVE, TCD, PVL and IAN. With a high level of dust production during its passage through the Solar System in the late 90's, it poses as a promising candidate, though more detailed modeling casts some doubt as to its potential as an immediate parent body for Earth-intersecting meteoroids Beech et al. (1996).

6. Conclusions

Using more than one million individual orbits measured in the southern hemisphere during 2012–2015 by SAAMER-OS radar we found 58 meteor showers through an algorithm based on a 3D wavelet searching method. We performed a detailed analysis of the ideal wavelet probe size using the SDA shower as a calibration source (Fig. 5) resulting in different settings than those used by B2010. The ideal angular probe size for SAAMER, $\sigma_\Lambda = \sigma_\beta = 2.5°$, is significantly smaller than for CMOR (4°, c.f. B2010), while the ideal velocity probe size for SAAMER $\sigma_{v_g} = 15\%$ is 50% larger than for CMOR (10%, c.f. B2010). With more than 20 showers observable by both SAAMER and CMOR, we will investigate this discrepancy in the future.

All meteor streams last for at least four days and were required to satisfy several criteria described in Section 4. In our study we found 34 new streams (see Table 2) and 24 streams (see Table 3) that were listed previous to this work on the IAU Meteor Shower Working list. Our approach is very similar to that used by B2010, although, somewhat more restrictive in several parameters.

Most of the 34 new meteor showers were found within the south toroidal source region, which is a less studied counterpart of the north toroidal source (Campbell-Brown and Wiegert, 2009; Janches et al., 2015). We also recognized one shower complex- Puppids-Pixidids Complex -in the south toroidal source containing 7 newly discovered showers. We also confirmed a Toroidal-Helion-Anti-helion linked radiant ring structure similar to that reported by B2010, extending it for the southern part thus completing the shower list for this ring for both hemispheres.

The majority of previously observed and new meteor showers have unknown parent bodies. We performed a simple parent body search using the method developed by Valsecchi et al. (1999) which provides a list of potential parent bodies for our showers (Tables 4 and 5). While several parent bodies have very promising orbital similarity with our meteor showers, to confirm their connection requires full-fledged modeling that is far beyond the scope of this manuscript.

We note that the geocentric velocities presented in this paper are not corrected for atmospheric deceleration, which can potentially change the value of the geocentric velocity for a significant fraction of the showers presented. Based on the experience gained with CMOR, this correction will tend to increase the geocentric velocity by a few percent (see Table 1). This change will result in a shift towards orbits with higher semimajor axes and eccentricities. A future focus for these streams will include measurement of their mass distribution indices (**?**).

Acknowledgements

PGB and PP thank the Canada Research Chair program, the Natural Sciences and Engineering Research Council and the NASA Meteoroid Environment Office for funding support under co-operative agreement NNX15AC94A. The deployment of SAAMER and its remote receiving stations, as well as the work presented in this paper, were supported by NSF awards AGS-0634650, AGS-0944104, and AST-0908118. DJ's participation is currently supported through NASA awards 12-PAST12-0007 and 12-PATM12-0006. The authors wish to give special thanks to the EARG personnel for their invaluable assistance with the operation and day-to-day oversight of SAAMER. Without their help, operating a system on the other side of the planet would be impossible!

References

Abedin, A., Wiegert, P., Pokorný, P., Brown, P., Jan. 2017. The age and the probable parent body of the daytime arietid meteor shower. Icarus, 281, 417–443.

Andreić, Ž., Gural, P., Šegon, D., Skokić, I., Korlević, K., Vida, D., Novoselnik, F., Gostinski, D., Jun. 2014. Results of CMN 2013 search for new showers across CMN and SonotaCo databases I-0.5mm. WGN, Journal of the International Meteor Organization 42, 90–97.

Babadzhanov, P. B., Obrubov, I. V., Mar. 1992. Evolution of short-period meteoroid streams. Celestial Mechanics and Dynamical Astronomy 54, 111–127.

Babadzhanov, P. B., Williams, I. P., Kokhirova, G. I., Jun. 2008a. Meteor showers associated with 2003EH1. Monthly Notices of the RAS, 386, 2271–2277.

Babadzhanov, P. B., Williams, I. P., Kokhirova, G. I., Feb. 2008b. Near-Earth asteroids among the Piscids meteoroid stream. Astronomy and Astrophysics, 479, 249–255.

Babadzhanov, P. B., Williams, I. P., Kokhirova, G. I., May 2008c. Near-Earth Objects in the Taurid complex. Monthly Notices of the RAS, 386, 1436–1442.

Baggaley, W. J., Bennett, R. G. T., Steel, D. I., Taylor, A. D., Sep. 1994. The Advanced Meteor Orbit Radar Facility - AMOR. Quarterly Journal of the RAS, 35, 293.

Beech, M., Brown, P., Jones, J., Nov. 1996. On the non-observability of meteors from Comet C/1995 01 Hale-Bopp. Monthly Notices of the RAS, 283, 137–140.

Bland, P. A., Spurný, P., Bevan, A. W. R., Howard, K. T., Towner, M. C., Benedix, G. K., Greenwood, R. C., Shrbený, L., Franchi, I. A., Deacon, G., Borovička, J., Ceplecha, Z., Vaughan, D., Hough, R. M., Mar. 2012. The Australian Desert Fireball Network: a new era for planetary science. Australian Journal of Earth Sciences 59, 177–187.

Brown, P., Jones, J., Weryk, R. J., Campbell-Brown, M. D., Dec. 2004. The Velocity Distribution of Meteoroids at the Earth as Measured by the Canadian Meteor Orbit Radar (CMOR). Earth Moon and Planets 95, 617–626.

Brown, P., Weryk, R. J., Wong, D. K., Jones, J., May 2008. A meteoroid stream survey using the Canadian Meteor Orbit Radar. I. Methodology and radiant catalogue. Icarus, 195, 317–339.

Brown, P., Wong, D. K., Weryk, R. J., Wiegert, P., May 2010. A meteoroid stream survey using the Canadian Meteor Orbit Radar. II: Identification of minor showers using a 3D wavelet transform. Icarus, 207, 66–81.

Bruzzone, J. S., Brown, P., Weryk, R. J., Campbell-Brown, M. D., Jan. 2015. A decadal survey of the Daytime Arietid meteor shower using the Canadian Meteor Orbit Radar. Monthly Notices of the RAS, 446, 1625–1640.

Burns, J. A., Lamy, P. L., Soter, S., Oct. 1979. Radiation forces on small particles in the solar system. Icarus, 40, 1–48.

Bus, S. J., Binzel, R. P., Jul. 2002. Phase II of the Small Main-Belt Asteroid Spectroscopic Survey. A Feature-Based Taxonomy. Icarus, 158, 146–177.

Campbell-Brown, M., Brown, P. G., Feb. 2015. A 13-year radar study of the η-Aquariid meteor shower. Monthly Notices of the RAS, 446, 3669–3675.

Campbell-Brown, M., Wiegert, P., Jan. 2009. Seasonal variations in the north toroidal sporadic meteor source. Meteoritics and Planetary Science 44, 1837–1848.

Campbell-Brown, M. D., Jul. 2008. High resolution radiant distribution and orbits of sporadic radar meteoroids. Icarus, 196, 144–163.

Chesley, S. R., Chodas, P. W., Milani, A., Valsecchi, G. B., Yeomans, D. K., Oct. 2002. Quantifying the Risk Posed by Potential Earth Impacts. Icarus, 159, 423–432.

Fritts, D. C., Janches, D., Hocking, W. K., Oct. 2010. Southern Argentina Agile Meteor Radar: Initial assessment of gravity wave momentum fluxes. Journal of Geophysical Research (Atmospheres) 115, D19123.

Fritts, D. C., Janches, D., Hocking, W. K., Mitchell, N. J., Taylor, M. J., May 2012. Assessment of gravity wave momentum flux measurement capabilities by meteor radars having different transmitter power and antenna configurations. Journal of Geophysical Research (Atmospheres) 117, D10108.

Galligan, D. P., Baggaley, W. J., 2002. Wavelet enhancement for detecting shower structure in radar meteoroid data II. Application to the AMOR data. In: Green, S. F., Williams, I. P., McDonnell, J. A. M., McBride, N.

(Eds.), IAU Colloq. 181: Dust in the Solar System and Other Planetary Systems. Vol. 15. p. 48.

Galligan, D. P., Baggaley, W. J., Sep. 2004. The orbital distribution of radar-detected meteoroids of the Solar system dust cloud. Monthly Notices of the RAS, 353, 422–446.

Hocking, W. K., Fuller, B., Vandepeer, B., Jan. 2001. Real-time determination of meteor-related parameters utilizing modern digital technology. Journal of Atmospheric and Solar-Terrestrial Physics 63, 155–169.

Hocking, W. K., Thayaparan, T., Jones, J., 1997. Meteor decay times and their use in determining a diagnostic mesospheric Temperature-pressure parameter: Methodology and one year of data. Geophysics Research Letters, 24, 2977–2980.

Janches, D., Close, S., Hormaechea, J. L., Swarnalingam, N., Murphy, A., O'Connor, D., Vandepeer, B., Fuller, B., Fritts, D. C., Brunini, C., Aug. 2015. The Southern Argentina Agile MEteor Radar Orbital System (SAAMER-OS): An Initial Sporadic Meteoroid Orbital Survey in the Southern Sky. Astrophysical Journal, 809, 36.

Janches, D., Hocking, W., Pifko, S., Hormaechea, J. L., Fritts, D. C., Brunini, C., Michell, R., Samara, M., Mar. 2014. Interferometric meteor head echo observations using the Southern Argentina Agile Meteor Radar. Journal of Geophysical Research (Space Physics) 119, 2269–2287.

Janches, D., Hormaechea, J. L., Brunini, C., Hocking, W., Fritts, D. C., Apr. 2013. An initial meteoroid stream survey in the southern hemisphere using the Southern Argentina Agile Meteor Radar (SAAMER). Icarus, 223, 677–683.

Jenniskens, J., Baggaley, J., Crumpton, I., Aldous, P., Gural, P. S., Samuels, D., Albers, J., Soja, R., Apr. 2016a. A surprise southern hemisphere meteor shower on New-Year's Eve 2015: the Volantids (IAU#758, VOL). WGN, Journal of the International Meteor Organization 44, 35–41.

Jenniskens, P., 2006. Meteor Showers and Their Parent Comets. Cambridge University Press.

Jenniskens, P., Duckworth, H., Grigsby, B., Jun. 2012. Daytime Arietids and Marsden Sunskirters (ARI, IAU #171). WGN, Journal of the International Meteor Organization 40, 98–100.

Jenniskens, P., Gural, P. S., Dynneson, L., Grigsby, B. J., Newman, K. E., Borden, M., Koop, M., Holman, D., Nov. 2011. CAMS: Cameras for Allsky Meteor Surveillance to establish minor meteor showers. Icarus, 216, 40–61.

Jenniskens, P., Nénon, Q., Mar. 2016. CAMS verification of single-linked high-threshold D-criterion detected meteor showers. Icarus, 266, 371–383.

Jenniskens, P., Nénon, Q., Albers, J., Gural, P. S., Haberman, B., Holman, D., Morales, R., Grigsby, B. J., Samuels, D., Johannink, C., Mar. 2016b. The established meteor showers as observed by CAMS. Icarus, 266, 331–354.

Jenniskens, P., Nénon, Q., Gural, P. S., Albers, J., Haberman, B., Johnson, B., Holman, D., Morales, R., Grigsby, B. J., Samuels, D., Johannink, C., Mar. 2016c. CAMS confirmation of previously reported meteor showers. Icarus, 266, 355–370.

Jenniskens, P., Nénon, Q., Gural, P. S., Albers, J., Haberman, B., Johnson, B., Morales, R., Grigsby, B. J., Samuels, D., Johannink, C., Mar. 2016d. CAMS newly detected meteor showers and the sporadic background. Icarus, 266, 384–409.

Jenniskens, P., Vaubaillon, J., Binzel, R. P., DeMeo, F. E., Nesvorný, D., Bottke, W. F., Fitzsimmons, A., Hiroi, T., Marchis, F., Bishop, J. L., Vernazza, P., Zolensky, M. E., Herrin, J. S., Welten, K. C., Meier, M. M. M., Shaddad, M. H., Oct. 2010. Almahata Sitta (=asteroid 2008 TC_3) and the search for the ureilite parent body. Meteoritics and Planetary Science 45, 1590–1617.

Jones, J., 1977. Meteor Radiant Distribution Using Spherical Harmonic Analysis. Bulletin of the Astronomical Institutes of Czechoslovakia 28, 272.

Jones, J., Brown, P., Dec. 1993. Sporadic meteor radiant distributions - Orbital survey results. Monthly Notices of the RAS, 265, 524.

Jones, J., Brown, P., Ellis, K. J., Webster, A. R., Campbell-Brown, M., Krzemenski, Z., Weryk, R. J., Apr. 2005. The Canadian Meteor Orbit Radar: system overview and preliminary results. Planetary Space Science, 53, 413–421.

Jones, J., Jones, W., Apr. 2006. Meteor radiant activity mapping using single-station radar observations. Monthly Notices of the RAS, 367, 1050–1056.

Jones, J., McIntosh, B. A., Hawkes, R. L., May 1989. The age of the Orionid meteoroid stream. Monthly Notices of the RAS, 238, 179–191.

Jones, W., Jul. 1997. Theoretical and observational determinations of the ionization coefficient of meteors. Monthly Notices of the RAS, 288, 995–1003.

Jopek, T. J., Kaňuchová, Z., Jul. 2014. Current status of the˜IAU MDC Meteor Showers Database. Meteoroids 2013, 353–364.

Jopek, T. J., Koten, P., Pecina, P., May 2010. Meteoroid streams identification amongst 231 Southern hemisphere video meteors. Monthly Notices of the RAS, 404, 867–875.

Kostolansky, E., Apr. 1998. On asteroidal meteoroid streams detection. Contributions of the Astronomical Observatory Skalnate Pleso 28, 22–30.

Lau, E. M., Avery, S. K., Avery, J. P., Janches, D., Palo, S. E., Schafer, R., Makarov, N. A., Jul. 2006. Statistical characterization of the meteor trail distribution at the South Pole as seen by a VHF interferometric meteor radar. Radio Science 41, RS4007.

Mattiazzo, M., Maury, A., Soulier, J.-F., Sato, H., Weryk, R., Guido, E., Howes, N., Jacques, C., Pimentel, E., Barros, J., Aug. 2015. Comet C/2015 P3 (Swan). Central Bureau Electronic Telegrams 4136.

Molau, S., Kerr, S., Apr. 2014. Meteor showers of the southern hemisphere. WGN, Journal of the International Meteor Organization 42, 68–75.

Molau, S., Rendtel, J., Aug. 2009. A Comprehensive List of Meteor Showers Obtained from 10 Years of Observations with the IMO Video Meteor Network. WGN, Journal of the International Meteor Organization 37, 98–121.

Nesvorný, D., Janches, D., Vokrouhlický, D., Pokorný, P., Bottke, W. F., Jenniskens, P., Dec. 2011. Dynamical Model for the Zodiacal Cloud and Sporadic Meteors. Astrophysical Journal, 743, 129.

Pokorný, P., Vokrouhlický, D., Nesvorný, D., Campbell-Brown, M., Brown, P., Jul. 2014. Dynamical Model for the Toroidal Sporadic Meteors. Astrophysical Journal, 789, 25.

Sekanina, Z., Feb. 1973. Statistical Model of Meteor Streams. III. Stream Search Among 19303 Radio Meteors. Icarus, 18, 253–284.

Sekanina, Z., Feb. 1976. Statistical model of meteor streams. IV - A study of radio streams from the synoptic year. Icarus, 27, 265–321.

SonotaCo, Apr. 2009. A meteor shower catalog based on video observations in 2007-2008. WGN, Journal of the International Meteor Organization 37, 55–62.

Towner, M. C., Bland, P. A., Cupak, M. C., Howie, R. M., Sansom, E. K., Paxman, J. P., Inie, M., Galloway, M., Deacon, G., Dyl, K. A., Benedix, G. K., Tingay, S. J., Harrison, J. A., Bevan, A. W. R., Mar. 2015. Initial Results from the Desert Fireball Network. In: Lunar and Planetary Science Conference. Vol. 46 of Lunar and Planetary Science Conference. p. 1693.

Valsecchi, G. B., Jopek, T. J., Froeschle, C., Apr. 1999. Meteoroid stream identification: a new approach - I. Theory. Monthly Notices of the RAS, 304, 743–750.

Warner, B. D., Jan. 2015. A Quartet of Near-Earth Asteroid Binary Canidates. Minor Planet Bulletin 42, 79–83.

Webster, A. R., Jones, J., Dec. 2004. Single and Multi-Station Radar Observations of the Geminid/sextantid Meteor Stream System. Earth Moon and Planets 95, 713–721.

Wiegert, P., Brown, P., Dec. 2005. The Quadrantid meteoroid complex. Icarus, 179, 139–157.

Wiesel, W., 1997. Spaceflight Dynamics. McGraw-Hill series in aeronautical and aerospace engineering. McGraw-Hill.

Wirström, E. S., Lerner, M. S., Källström, P., Levinsson, A., Olivefors, A., Tegehall, E., Apr. 2016. HCN observations of comets C/2013 R1 (Lovejoy) and C/2014 Q2 (Lovejoy). Astronomy and Astrophysics, 588, A72.

Younger, J. P., Reid, I. M., Vincent, R. A., Holdsworth, D. A., Murphy, D. J., Sep. 2009. A southern hemisphere survey of meteor shower radiants and associated stream orbits using single station radar observations. Monthly Notices of the RAS, 398, 350–356.

Table 2: Showers found using our search algorithm associated with showers in IAU Meteor Shower list sorted by the time of the solar longitude of their peak activity $\lambda_{\max}$. Note that two showers, MHY and DCS, have two entries in this table. Both showers exhibit two distinctive peaks in activity separated by several days and by several degrees in the angular space. For each shower we provide the solar longitude of the beginning of the shower ($\lambda_{\rm beg}$), the solar longitude of the peak ($\lambda_{\max}$), the solar longitude of the end of the shower ($\lambda_{\rm end}$), the duration of the shower in degrees, the sun-centered longitude ($\lambda - \lambda_0$), the sun-centered latitude (β), the geocentric right ascension (RA), the geocentric declination (Dec), the geocentric velocity (V_g), the wavelet coefficient at the peak ($W_{c_{\max}}$), the number of σ values above the annual median ($\sigma_{\rm wave}$), the number of radiants used for determination of the wavelet coefficient ($r_{\rm cnt}$), the drift in RA per degree of the solar longitude ($\mathrm{RA}_{\rm dr}$), the error of the drift in RA, the correlation coefficient of the linear fit to the drift ($r_{\rm RA}$), the drift in Dec per degree of the solar longitude ($\mathrm{Dec}_{\rm dr}$), the error of the drift in Dec, the correlation coefficient of the linear fit to the drift ($r_{\rm Dec}$), the semimajor axis (a) with its uncertainty, the eccentricity (e) with its uncertainty, the inclination (I) with its uncertainty, the argument of pericenter (ω) with its uncertainty, the longitude of the ascending node (Ω) with its uncertainty, the perihelion distance (q) with its uncertainty, and the Tisserand parameter with respect to the Jupiter ($T_{\rm J}$).

Name	IAU	$\lambda_{\rm start}$	$\lambda_{\max}$	$\lambda_{\rm end}$	Dur.	$\lambda-\lambda_0$	β	RA	Dec	$V_{\rm g}$	$W_{c_{\max}}$	$\sigma_{\rm wave}$	$r_{\rm cnt}$	$RA_{\rm dr}$	±	$r_{\rm RA}$	$\mathrm{Dec}_{\rm dr}$	±	$r_{\rm Dec}$	a	±	e	±	I	±	ω	±	Ω	q	±	$T_{\rm j}$
η Aquariids	ETA	33	46	60	28	293.7	7.2	338.5	-1.2	64.2	475.0	52.2	433	0.70	0.02	0.989	0.34	0.01	0.993	4.78	6.26	0.886	0.136	164.3	2.3	91.3	12.8	46	0.545	0.071	0.2
Southern Daytime ω-Cetids	OCE	21	47	61	41	330.4	-13.8	21.3	-5.9	36.5	334.9	26.8	331	0.91	0.02	0.992	0.48	0.01	0.989	1.57	0.25	0.916	0.019	35.8	4.0	215.0	2.0	227	0.132	0.015	3.7
Daytime Arietids	ARI	73	79	81	9	331.5	7.2	46.0	24.9	40.5	64.0	6.5	55	0.89	0.04	0.996	0.05	0.08	0.263	2.48	0.79	0.969	0.014	26.7	4.7	28.5	2.2	79	0.077	0.014	2.4
Southern June Aquilids	SZC	76	80	82	7	218.9	-13.5	304.3	-33.6	35.9	446.1	34.6	463	0.17	0.03	0.926	0.40	0.05	0.964	1.00	0.08	0.924	0.014	48.6	6.2	158.0	1.6	260	0.076	0.010	5.5
Southern May Ophiuchids	SOP	63	81	96	34	188.3	-6.3	269.2	-29.7	25.9	221.7	15.0	261	0.91	0.02	0.995	-0.11	0.01	0.829	2.00	0.28	0.784	0.035	6.3	1.1	107.9	2.2	261	0.432	0.020	3.4
Northern June Aquilids	NZC	84	101	116	33	210.4	13.5	310.1	-4.4	36.5	189.5	19.2	258	0.78	0.02	0.994	0.19	0.02	0.894	1.46	0.21	0.916	0.018	36.8	4.2	327.1	2.0	101	0.123	0.014	3.9
Microscopiids	MIC	83	104	120	38	208.5	-13.3	319.3	-29.7	35.9	212.2	15.1	332	0.92	0.01	0.998	0.26	0.01	0.969	1.55	0.23	0.911	0.019	33.2	3.7	144.4	2.0	284	0.138	0.015	3.7
Piscis Austrinids	PAU	122	125	134	13	215.3	-19.5	349.9	-25.6	39.9	252.6	17.4	703	0.72	0.06	0.973	0.39	0.06	0.905	1.58	0.29	0.910	0.017	60.3	5.2	143.5	2.6	305	0.143	0.013	3.5
Southern δ Aquariids	SDA	111	125	161	51	209.5	-7.5	339.2	-16.8	39.9	3296	141	2180	0.79	0.01	0.996	0.29	0.01	0.972	2.08	0.53	0.965	0.014	27.8	4.9	152.8	2.2	305	0.074	0.013	2.8
α Capricornids	CAP	105	127	131	27	178.6	9.7	305.6	-9.4	24.4	139.6	16.3	106	0.60	0.02	0.988	0.21	0.01	0.959	3.59	0.97	0.840	0.045	7.9	0.9	266.9	2.0	127	0.577	0.017	2.3
Northern δ Aquariids	NDA	131	136	142	12	210.3	7.7	344.4	1.7	38.1	80.7	7.0	142	0.69	0.02	0.998	0.08	0.06	0.429	1.66	0.30	0.953	0.015	26.5	4.5	332.9	2.0	136	0.079	0.014	3.4
Daytime Sextantids	DSX	175	187	197	23	330.8	-11.0	155.4	-1.6	31.4	369.7	29.9	271	0.52	0.04	0.954	-0.54	0.02	0.989	1.08	0.08	0.858	0.022	22.2	2.7	213.6	1.8	7	0.154	0.017	5.2
October Leporids	OLP	192	199	204	13	236.8	-40.8	78.7	-17.9	26.7	101.2	11.8	161	1.13	0.08	0.981	0.32	0.06	0.886	0.76	0.02	0.549	0.017	53.4	3.2	149.0	2.7	19	0.341	0.019	7.3
Orionids	ORI	204	207	214	11	248.3	-8.3	95.5	15.1	64.2	61.7	7.6	50	0.77	0.05	0.983	-0.09	0.05	0.512	3.24	2.83	0.823	0.134	162.5	2.2	86.5	13.8	27	0.574	0.073	0.7
β Canis Majorids	MCB	234	236	239	6	217.7	-44.8	92.8	-21.3	42.3	77.8	7.2	193	2.07	0.23	0.977	-0.46	0.30	0.611	4.75	3.34	0.873	0.086	68.5	2.7	80.6	5.0	56	0.603	0.024	1.4
November ω Orionids	NOO	241	248	252	12	205.3	-9.0	93.4	14.4	41.7	96.6	9.8	129	0.90	0.09	0.951	-0.06	0.03	0.501	4.68	3.17	0.976	0.018	27.4	3.9	142.7	2.4	68	0.112	0.015	1.5
e Velids	EVE	240	250	261	22	269.9	-62.0	131.4	-48.2	39.9	280.3	13.6	739	0.67	0.06	0.931	-0.38	0.04	0.892	2.08	0.53	0.525	0.121	71.9	2.3	1.4	3.1	70	0.986	0.000	2.8
σ Serpentids	SSE	259	274	295	37	326.6	18.0	242.1	-2.6	42.3	103.2	14.5	200	0.89	0.03	0.987	-0.22	0.03	0.815	2.01	0.54	0.933	0.019	58.1	5.3	37.8	2.7	274	0.134	0.013	2.8
December Hydrids	DHY	272	275	277	6	230.4	-30.5	137.4	-15.7	49.9	40.0	6.9	108	0.61	0.14	0.905	-0.85	0.11	0.969	2.22	0.85	0.825	0.053	96.3	3.7	109.9	7.8	95	0.387	0.04	2.3
α Hydrids	AHY	272	284	294	23	208.4	-25.8	127.8	-7.7	42.3	100.3	13.1	138	0.58	0.02	0.986	-0.08	0.04	0.439	4.56	3.06	0.94	0.039	56.6	3.6	119.4	3.5	104	0.273	0.018	1.5
Daytime ξ Sagittariids	XSA	270	288	297	28	353.1	6.7	281.5	-16.2	25.5	313.6	20.9	419	0.89	0.02	0.995	0.06	0.01	0.669	2.13	0.32	0.784	0.036	6.3	1.0	77.8	2.1	288	0.460	0.019	3.2
Daytime χ Capricornids	DCS	281	299	299	19	0.8	-9.5	304.2	-29.5	23.7	202.2	16.3	176	1.10	0.04	0.990	0.19	0.03	0.829	2.94	0.61	0.805	0.043	7.3	0.8	273.8	2.0	119	0.574	0.016	2.7
μ Hydrids	MHY	298	303	309	12	228.1	-32.3	158.3	-25.9	35.4	118.3	12.4	268	0.83	0.07	0.988	-0.46	0.28	0.634	0.9	0.06	0.699	0.016	67.1	4.0	139.8	3.8	123	0.270	0.021	6.0
Daytime χ Capricornids	DCS	302	305	316	15	356.4	-8.5	305.7	-28.1	24.4	180.1	11.2	265	0.70	0.05	0.968	0.29	0.02	0.971	2.37	0.39	0.783	0.039	7.2	0.9	264.9	2.1	125	0.513	0.018	3.0
μ Hydrids	MHY	300	310	310	11	221.1	-24.0	162.1	-18.5	36.5	166.6	17.0	287	0.66	0.14	0.866	0.03	0.09	0.127	0.99	0.08	0.825	0.016	60.7	4.7	145.3	2.6	130	0.173	0.014	5.5
α Antilids	AAN	301	312	324	24	214.8	-19.5	160.2	-12.7	41.1	210.6	19.1	328	0.60	0.03	0.981	-0.36	0.06	0.851	1.61	0.31	0.91	0.018	59.4	5.1	142.1	2.7	132	0.146	0.013	3.5

Table 3: The same as Table 2 but now for new showers found using our search algorithm sorted by the time of the solar longitude of their peak activity λ_{max}.

Name	IAU	λ_{start}	λ_{max}	λ_{end}	Dur.	$\lambda-\lambda_0$	β	RA	Dec	V_g	$W_{c_{max}}$	σ_{wave}	r_{cnt}	RA_{dr}	±	r_{RA}	Dec_{dr}	±	r_{Dec}	a	±	e	±	I	±	ω	±	Ω	q	±	T_j
30 Ophiuchids	THO	5	8	9	5	248.5	18.7	257.2	-4.1	57.0	26.0	6.5	62	0.90	0.23	0.916	1.57	0.16	0.985	1.36	0.37	0.615	0.051	138.1	2.9	284.5	16.0	8	0.523	0.084	3.2
Octantids	OCD	21	26	40	20	252.9	-54.8	294.1	-77.4	31.9	133.4	10.8	257	2.61	0.18	0.963	0.41	0.04	0.925	0.97	0.06	0.174	0.021	65.1	2.8	112.7	20.2	206	0.797	0.062	5.7
ρ Phoenicids	RPH	34	38	43	10	308.2	-49.3	14.0	-49.2	43.0	191.5	20.9	233	0.89	0.04	0.990	0.50	0.11	0.854	2.70	1.04	0.726	0.098	77.0	2.6	291.6	6.6	218	0.739	0.028	2.2
o Pavonids	OPA	45	46	49	5	246.4	-50.0	315.5	-69.9	31.0	79.3	7.1	220	0.21	0.55	0.212	-0.02	0.34	0.032	0.88	0.04	0.312	0.026	64.5	3.0	133.6	8.9	226	0.604	0.049	6.3
υ Pavonids	UPA	54	54	61	8	237.8	-44.8	309.0	-65.3	31.0	58.7	6.1	155	1.02	0.20	0.933	0.69	0.17	0.896	0.86	0.04	0.452	0.020	63.5	3.2	135.8	5.8	234	0.470	0.035	6.4
Telescopiids	TEL	57	63	66	10	221.4	-31.3	291.0	-53.6	31.9	59.8	6.4	146	2.51	0.26	0.965	-0.27	0.11	0.657	0.94	0.05	0.710	0.018	55.5	3.6	139.5	3.0	243	0.273	0.017	5.9
α Sagittariids	ASG	78	78	82	5	212.2	-19.5	295.6	-41.2	30.5	80.3	6.2	345	2.38	0.38	0.975	-0.01	0.14	0.058	1.03	0.07	0.812	0.021	36.0	3.2	143.8	1.8	258	0.193	0.015	5.5
β Aquilids	BAD	80	81	87	8	220.7	25.0	298.5	4.6.0	31.0	30.3	6.5	58	0.90	0.16	0.940	0.05	0.15	0.149	0.88	0.04	0.783	0.017	49.9	4.0	328.1	2.0	81	0.191	0.014	6.2
α Phoenicids	APH	97	101	102	6	243.8	-38.3	4.3	-40.5	27.1	55.2	7.2	121	0.66	0.09	0.974	0.66	0.08	0.977	0.70	0.01	0.597	0.019	58.6	3.7	159.3	2.1	281	0.281	0.018	7.8
ζ Phoenicids	ZPH	96	105	108	13	237.5	-52.0	13.7	-52.8	41.7	168.8	13.1	361	0.84	0.09	0.946	0.42	0.05	0.939	2.14	0.60	0.616	0.099	76.9	2.6	60.3	7.2	285	0.821	0.027	2.7
ψ Phoenicids	PPH	98	111	120	23	251.3	-53.8	30.1	-46.9	37.6	432.7	26.2	673	0.84	0.03	0.990	0.59	0.02	0.987	1.26	0.15	0.291	0.064	74.8	2.7	63.3	14.7	291	0.890	0.035	4.4
λ Caelids	LCA	193	195	196	4	232.9	-55.3	75.2	-32.9	40.5	101.8	7.0	304	-0.02	0.50	0.031	0.73	0.39	0.798	2.67	0.93	0.693	0.102	71.1	2.4	55.5	5.6	15	0.822	0.021	2.3
σ Columbids	SCO	198	199	203	6	250.0	-53.8	89.3	-30.3	39.3	108.7	7.9	350	0.11	0.08	0.590	0.42	0.27	0.615	1.39	0.21	0.370	0.079	75.8	2.7	57.0	11.2	19	0.875	0.029	4.0
γ Sextantids	GSE	196	199	199	4	316.9	-20.8	150.1	-10.0	27.5	45.4	6.2	95	1.00	0.40	0.867	-0.60	0.21	0.896	0.74	0.02	0.792	0.019	38.4	3.6	204.0	1.3	19	0.154	0.013	7.4
3 Puppids	THP	192	200	205	14	287.2	-53.8	115.4	-33.5	32.9	82.8	7.8	281	1.08	0.10	0.959	0.03	0.06	0.157	0.96	0.06	0.183	0.021	67.0	2.8	248.5	20.2	20	0.787	0.063	5.7
η Canis Majorids	ECM	200	201	206	7	276.8	-55.8	108.4	-34.1	33.9	100.7	7.0	381	0.11	0.13	0.354	0.03	0.31	0.048	1.02	0.08	0.061	0.030	68.7	2.7	284.1	65.2	21	0.954	0.051	5.4
October β Pyxidids	OBP	203	207	208	6	295.5	-51.8	126.8	-34.8	33.4	68.6	6.9	225	0.53	0.19	0.851	-0.10	0.05	0.753	0.99	0.07	0.284	0.019	66.7	2.8	252.1	13.3	27	0.708	0.050	5.6
October α Pyxidids	OAP	206	211	221	16	301.3	-48.8	135.2	-34.6	32.4	72.5	7.4	211	0.60	0.20	0.660	0.08	0.06	0.347	0.94	0.06	0.369	0.019	64.3	2.9	240.5	8.9	31	0.594	0.042	5.9
October Puppids	OPU	208	212	216	9	289.3	-53.8	125.0	-36.4	31.9	73.2	7.0	273	-0.16	0.19	0.325	-0.13	0.11	0.431	0.94	0.06	0.206	0.022	64.7	2.8	243.4	16.4	32	0.748	0.058	5.9
ζ Antliids	ZAN	207	212	214	8	307.1	-42.5	143.5	-31.0	32.4	56.3	6.8	180	0.89	0.12	0.955	-0.27	0.20	0.519	0.89	0.05	0.505	0.018	63.5	3.2	229.2	5.6	32	0.443	0.031	6.1
October λ Velids	OLV	217	221	222	6	291.0	-52.8	132.8	-38.1	33.9	65.1	7.0	163	1.39	0.33	0.905	-0.45	0.12	0.873	0.99	0.07	0.231	0.020	68.0	2.8	256.3	17.1	41	0.762	0.054	5.6
November Puppids	NPU	220	224	225	6	280.4	-57.5	125.1	-40.5	35.4	137.3	9.6	451	1.41	0.13	0.987	-0.51	0.10	0.951	1.17	0.12	0.176	0.073	69.2	2.6	322.6	15.4	44	0.961	0.016	4.8
November λ Velids	NLV	226	232	237	12	284.9	-57.8	132.9	-43.8	36.5	96.3	6.8	256	-0.01	0.09	0.022	-0.29	0.08	0.787	1.28	0.15	0.265	0.080	69.9	2.6	320.2	11.0	52	0.941	0.017	4.4
ι Arids	IAD	247	250	251	5	13.8	-25.0	261.5	-48.3	21.3	44.7	8.0	47	1.24	0.76	0.758	-0.30	0.28	0.607	5.44	2.10	0.860	0.055	14.5	0.8	300.6	1.5	70	0.762	0.011	2.0
ι Lupids	ILU	267	271	272	6	316.5	-30.8	213.0	-46.1	37.0	71.8	9.3	185	1.58	0.35	0.912	-0.36	0.13	0.820	1.05	0.10	0.744	0.018	66.2	4.0	225.1	3.9	91	0.268	0.020	5.2
θ Carinids	TCD	274	276	280	7	282.3	-60.3	156.8	-59.2	41.7	172.4	9.8	581	2.13	0.26	0.964	-0.13	0.10	0.475	2.38	0.76	0.595	0.129	74.5	2.4	342.2	3.7	96	0.966	0.006	2.5
κ Velids	KVE	272	276	286	15	257.8	-60.5	141.1	-51.0	40.5	440.7	23.5	806	1.24	0.13	0.952	-0.48	0.07	0.905	2.08	0.54	0.536	0.120	72.9	2.4	19.1	4.1	96	0.965	0.007	2.8
6 Puppids	SXP	275	277	279	5	209.4	-37.0	119.7	-17.2	39.9	67.4	7.2	167	0.47	0.37	0.597	-0.22	0.18	0.584	3.72	1.85	0.876	0.059	58.6	2.8	98.0	4.2	97	0.460	0.021	1.8
Volantids	VOL	274	280	283	10	303.7	-77.8	121.1	-72.7	29.6	280.4	19.7	398	-1.42	0.39	0.787	-0.64	0.08	0.944	2.72	0.65	0.642	0.086	49.1	1.8	346.7	2.1	100	0.973	0.003	2.6
9 Herculids	NHR	281	282	285	5	318.3	25.0	243.2	4.3	38.1	51.8	9.9	105	0.04	0.12	0.215	-0.34	0.14	0.821	1.08	0.11	0.826	0.016	65.6	4.7	37.8	3.1	282	0.187	0.016	5.0
January μ Velids	JMV	282	287	296	15	268.6	-50.8	166.0	-51.1	34.9	145.5	9.8	339	0.92	0.09	0.945	-0.13	0.04	0.663	0.88	0.05	0.117	0.068	73.1	3.0	172.4	10.6	107	0.779	0.108	6.1
ψ Velids	PVL	278	288	298	21	238.4	-53.0	142.6	-42.6	41.7	170.0	12.5	383	1.05	0.04	0.986	-0.45	0.03	0.969	2.00	0.52	0.594	0.098	75.0	2.6	57.6	7.0	108	0.813	0.024	2.9
ι Antliids	IAN	299	302	304	6	239.3	-39.5	162.9	-36.2	36.5	63.2	6.8	265	0.06	0.2	0.169	-0.73	0.20	0.901	0.86	0.06	0.523	0.021	75.4	3.6	133.8	6.6	122	0.412	0.039	6.2
March β Equuleids	MBE	354	359	2	9	326.0	19.2	320.9	5.0	45.6	30.2	6.3	61	-0.01	0.00	0.868	-0.01	0.00	0.875	4.17	2.81	0.965	0.023	68.8	5.4	42.8	3.4	359	0.148	0.015	1.4

Table 4: Previously recognized showers found using our search algorithm sorted by the time of the solar longitude of their peak activity $\lambda_{\max}$.

Shower Name	IAU	Parent 1	H	D_N	Parent 2	H	D_N	Parent 3	H	D_N	Largest Parent	H	D_N	U	$\cos(\theta)$
η Aquariids	ETA	1P/Halley	5.5	0.0517	P/2010 H3 (SOHO)	—	1.0449	2015 DU180	20.8	1.3317	1P/Halley	5.5	0.0517	2.1778	-0.9073
Southern Daytime ω-Cetids	OCE	2013 KN6	18.5	0.0393	2015 DU180	20.8	0.0721	2014 JO25	18.1	0.1077	P/2010 H3 (SOHO)	—	0.3665	1.2440	-0.4761
Daytime Arietids	ARI	P/2010 H3 (SOHO)	—	0.0085	1998 QS52	14.3	0.1642	(1566) Icarus	16.9	0.1830	P/2010 H3 (SOHO)	—	0.0085	1.3790	-0.4731
Southern June Aquilids	SZC	(329915) 2005 MB	17.1	0.0926	(1566) Icarus	16.9	0.0937	P/2010 H3 (SOHO)	—	0.1092	P/2010 H3 (SOHO)	—	0.1092	1.2224	-0.6112
Southern May Ophiuchids	SOP	2008 XM1	22.0	0.0114	2009 XT6	20.2	0.0137	2004 LC2	18.5	0.0212	300P/Catalina	18.3	0.4425	0.8688	-0.1467
Northern June Aquilids	NZC	2015 NF	19.6	0.0786	2013 LC7	19.4	0.0962	2003 NC	19.4	0.1002	P/2010 H3 (SOHO)	—	0.2308	1.2405	-0.4932
Microscopiids	MIC	2015 NF	19.6	0.0570	2003 NC	19.4	0.0740	2013 LC7	19.4	0.1071	P/2010 H3 (SOHO)	—	0.2791	1.2229	-0.4664
Piscis Austrinids	PAU	2009 OG	16.2	0.0878	2014 LJ21	16.0	0.1423	2002 PM6	17.7	0.1570	C/2015 D4 (Borisov)	9.4	0.6133	1.3604	-0.5453
Southern δ Aquariids	SDA	2002 PM6	17.7	0.1098	2001 VB	18.4	0.1159	2004 QX2	21.7	0.1183	P/2010 H3 (SOHO)	—	0.6393	1.3602	-0.4892
α Capricornids	CAP	2015 PU228	20.3	0.0237	2014 OW3	22.4	0.0279	2008 BC15	26.6	0.0312	C/2007 W1 (Boattini)	12.0	0.4635	0.8276	0.0221
Northern δ Aquariids	NDA	2004 QX2	21.7	0.0326	2011 GS60	19.0	0.0731	2014 QO390	21.1	0.0851	C/2012 F6 (Lemmon)	5.5	0.8990	1.3034	-0.4992
Daytime Sextantids	DSX	2006 SO198	23.9	0.0490	2008 SC	21.7	0.0739	2006 KK21	20.4	0.0828	35/P Herschel	8.3	0.7615	1.0419	-0.4854
October Leporids	OLP	2009 UY17	20.9	0.1151	2015 TD323	19.9	0.1249	2009 HE	21.3	0.1267	35/P Herschel	8.3	0.4692	0.9030	-0.6263
Orionids	ORI	C/2010 L5 (WISE)	17.4	0.2049	55P/Tempel-Tuttle	10.0	0.7275	2004 UL	18.8	1.1655	C/2010 L5 (WISE)	17.4	0.2049	2.1545	-0.9168
β Canis Majorids	MCB	1998 KO3	19.5	0.0838	2010 US7	19.0	0.1169	C/2013 R1 (Lovejoy)	11.6	0.1177	C/2013 R1 (Lovejoy)	11.6	0.1177	1.4179	-0.4305
November ω Orionids	NOO	2013 WM	23.8	0.0974	2008 XM	20.0	0.1107	2011 WN15	19.6	0.1265	C/2013 R1 (Lovejoy)	11.6	0.7808	1.3964	-0.4166
e Velids	EVE	2006 BZ7	17.5	0.0696	2015 XG261	23.1	0.0926	2010 XA68	21.9	0.1345	C/2013 R1 (Lovejoy)	11.6	0.1779	1.3253	-0.4668
σ Serpentids	SSE	2011 XA3	20.4	0.0597	(3200) Phaethon	14.6	0.1336	2011 WN15	19.6	0.1913	C/2013 R1 (Lovejoy)	11.6	0.6857	1.4012	-0.5213
December Hydrids	DHY	2012 MS4	18.7	0.2186	C/1995 OP (Hale-Bopp)	2.3	0.3568	C/2013 R1 (Lovejoy)	11.6	0.4861	C/1995 O1 (Hale-Bopp)	2.3	0.3568	1.6536	-0.6606
α Hydrids	AHY	2011 XA3	20.4	0.1562	2010 BG2	19.9	0.2074	2004 XK50	19.3	0.2488	C/2013 R1 (Lovejoy)	11.6	0.6691	1.4066	-0.4258
Daytime ξ Sagittariids	XSA	2013 AB65	27.6	0.0171	2005 AD13	17.9	0.0216	2015 AR45	19.8	0.0307	141P/Machholz	15.0	0.7390	0.8541	-0.1165
Daytime χ Capricornids	DCS	2011 OF26	24.8	0.0115	2012 BL14	28.2	0.0190	2016 BN14	26.5	0.0287	141P/Machholz	15.0	0.9158	0.8012	0.0112
μ Hydrids	MHY	2009 AE16	18.7	0.1101	2005 AC	18.2	0.1621	2010 BG2	19.9	0.1848	C/2009 O2 (Catalina)	12.3	0.6501	1.1666	-0.6309
Daytime χ Capricornids	DCS	2011 OF26	24.8	0.0119	2011 CT4	20.5	0.0138	2011 BW10	25.2	0.0147	(1685) Toro	14.2	0.5164	0.8234	-0.0607
μ Hydrids	MHY	2010 BG2	19.9	0.0764	2010 CC19	22.3	0.0914	2009 AE16	18.7	0.1063	C/2009 O2 (Catalina)	12.3	0.7319	1.1998	-0.6041
α Antilids	AAN	2010 BG2	19.9	0.0567	2006 AL8	18.4	0.1154	2002 AJ129	18.7	0.1337	C/2009 O2 (Catalina)	12.3	0.6708	1.3577	-0.5393

Table 5: New showers found using our search algorithm sorted by the time of the solar longitude of their peak activity $\lambda_{\max}$.

Shower Name	IAU	Parent 1	H	D_N	Parent 2	H	D_N	Parent 3	H	D_N	Largest Parent	H	D_N	U	$\cos(\theta)$
30 Ophiuchids	THO	2012 US136	15.9	0.6771	2012 FZ23	18.2	0.8639	2010 EF44	20.2	0.9269	2012 US136	15.9	0.6771	1.9062	-0.8837
Octantids	OCD	2015 TT178	20.7	0.0934	2004 HC2	19.5	0.1168	2002 TE66	18.4	0.1459	1998 XM4	15.5	0.2909	1.0735	-0.5511
ρ Phoenicids	RPH	2002 TW55	18.0	0.0994	2001 TZ44	17.4	0.1823	2007 VG	21.0	0.2091	C/2015 P3 (Swan)	12.5	0.8117	1.4564	-0.5121
o Pavonids	OPA	1998 XM4	15.5	0.0986	2007 TD71	18.4	0.1003	(5381) Sekhmet	16.6	0.1079	C/2015 P3 (Swan)	12.5	0.7877	1.0470	-0.5886
υ Pavonids	UPA	(5381) Sekhmet	16.6	0.0764	2001 TZ44	17.4	0.1393	2005 XN4	19.8	0.1503	C/2015 P3 (Swan)	12.5	0.5433	1.0483	-0.6018
Telescopiids	TEL	2010 SG13	18.3	0.1170	2003 HA	16.5	0.1296	2005 LX36	20.8	0.1439	C/2015 P3 (Swan)	12.5	0.3894	1.0783	-0.5688
α Sagittariids	ASG	2010 SG13	18.3	0.0285	(329915) 2005 MB	17.1	0.0399	(1566) Icarus	16.9	0.0533	P/2010 H3 (SOHO)	—	0.2668	1.0347	-0.5033
β Aquilids	BAD	(329915) 2005 MB	17.1	0.0292	2003 OS13	17.4	0.0713	2010 SG13	18.3	0.0716	C/2015 P3 (Swan)	12.5	0.3238	1.0545	-0.5919
α Phoenicids	APH	2006 AD	16.7	0.1679	2012 XT134	19.0	0.1683	2010 JU39	19.6	0.1732	C/2015 P3 (Swan)	12.5	0.3786	0.9338	-0.6964
ζ Phoenicids	ZPH	(5496) 1973 NA	16.0	0.0323	2012 XT134	19.0	0.1041	C/2015 D4 (Borisov)	9.4	0.1525	C/2015 D4 (Borisov)	9.4	0.1525	1.4179	-0.5211
ψ Phoenicids	PPH	(5496) 1973 NA	16.0	0.0600	C/2015 D4 (Borisov)	9.4	0.1793	2012 XT134	19.0	0.1884	C/2015 D4 (Borisov)	9.4	0.1793	1.2819	-0.5605
λ Caelids	LCA	2009 VQ25	18.6	0.0445	2010 QE2	17.2	0.0684	2009 FG1	18.8	0.0945	C/2015 P3 (Swan)	12.5	0.1044	1.3647	-0.4532
σ Columbids	SCO	2003 UL9	22.4	0.0713	2009 VQ25	18.6	0.0743	2009 FG1	18.8	0.0750	C/2015 P3 (Swan)	12.5	0.1295	1.3203	-0.5539
γ Sextantids	GSE	2001 TD45	19.9	0.0658	1999 VO6	17.0	0.0721	2004 VG64	18.3	0.0786	35/P Herschel	8.3	0.7429	0.9086	-0.6476
3 Puppids	THP	2003 UL9	22.4	0.0098	2009 FG1	18.8	0.0811	2009 VQ25	18.6	0.0832	C/2015 P3 (Swan)	12.5	0.2842	1.0980	-0.5680
η Canis Majorids	ECM	2003 UL9	22.4	0.0442	2009 FG1	18.8	0.1126	2003 QQ47	17.4	0.1479	C/2015 P3 (Swan)	12.5	0.3264	1.1346	-0.5586
October β Pyxidids	OBP	2003 UL9	22.4	0.0109	2009 VQ25	18.6	0.0856	2011 BJ2	18.2	0.1006	C/2015 P3 (Swan)	12.5	0.1944	1.1114	-0.5602
October α Pyxidids	OAP	2003 UL9	22.4	0.0440	2011 BJ2	18.2	0.0803	2008 HD3	19.8	0.0809	C/2015 P3 (Swan)	12.5	0.2057	1.0745	-0.5670
October Puppids	OPU	2003 UL9	22.4	0.0256	2007 HX4	17.7	0.0617	2014 HM129	20.3	0.0814	C/2015 P3 (Swan)	12.5	0.2619	1.0608	-0.5605
ζ Antliids	ZAN	2000 JE5	19.1	0.1005	2008 HD3	19.8	0.1097	2003 UL9	22.4	0.1238	C/2015 P3 (Swan)	12.5	0.2324	1.0723	-0.5938
October λ Velids	OLV	2007 HX4	17.7	0.0412	2011 WO4	19.2	0.0440	(10563) Izhdubar	16.8	0.0801	C/2015 P3 (Swan)	12.5	0.2250	1.1245	-0.5668
November Puppids	NPU	2011 WO4	19.2	0.0697	2007 HX4	17.7	0.0738	(10563) Izhdubar	16.8	0.0967	C/2015 P3 (Swan)	12.5	0.2691	1.1786	-0.5277
November λ Velids	NLV	(10563) Izhdubar	16.8	0.0455	2011 WO4	19.2	0.0619	2007 HX4	17.7	0.0966	C/2013 R1 (Lovejoy)	11.6	0.2748	1.2120	-0.5158
ι Arids	IAD	141P/Machholz	XXX	0.0105	2013 WS67	23.3	0.0303	2015 FH120	18.7	0.0334	141P/Machholz	15.0	0.0105	0.7153	0.2129
ι Lupids	ILU	2012 MS4	18.7	0.1077	2002 AB29	17.9	0.1396	2004 XK50	19.3	0.1427	C/2013 R1 (Lovejoy)	11.6	0.3701	1.2227	-0.5919
κ Velids	KVE	(2102) Tantalus	16.0	0.0506	2006 BZ7	17.5	0.0666	C/1995 O1 (Hale-Bopp)	2.3	0.1731	C/1995 O1 (Hale-Bopp)	2.3	0.1731	1.3428	-0.4781
θ Carinids	TCD	(2102) Tantalus	16.0	0.0695	2006 BZ7	17.5	0.0782	C/1995 O1 (Hale-Bopp)	2.3	0.1410	C/1995 O1 (Hale-Bopp)	2.3	0.1410	1.3846	-0.4829
6 Puppids	SXP	2002 AB29	17.9	0.0989	2012 MS4	18.7	0.1025	2004 XK50	19.3	0.1409	C/2013 R1 (Lovejoy)	11.6	0.3512	1.3273	-0.3882
Volantids	VOL	2011 AL1	19.6	0.0912	2008 CM	17.2	0.1013	(2102) Tantalus	16.0	0.1154	C/2013 R1 (Lovejoy)	11.6	0.5155	0.9882	-0.1741
9 Herculids	NHR	2011 XA3	20.4	0.1624	2004 XK50	19.3	0.1860	2002 AB29	17.9	0.2491	C/2013 R1 (Lovejoy)	11.6	0.6475	1.2610	-0.6011
January μ Velids	JMV	—	—	—	—	—	—	—	—	—	—	—	—	1.1498	-0.6342
ψ Velids	PVL	2008 AH4	21.6	0.0431	C/1995 O1 (Hale-Bopp)	2.3	0.1488	(2102) Tantalus	16.0	0.1498	C/1995 O1 (Hale-Bopp)	2.3	0.1488	1.3824	-0.5104
ι Antliids	IAN	2008 AH4	21.6	0.0922	2005 AC	18.2	0.2109	2005 OU2	19.1	0.2168	C/1995 O1 (Hale-Bopp)	2.3	0.4828	1.1995	-0.6676
March β Equuleids	MBE	2012 US136	15.9	0.1158	2010 EF44	20.2	0.1341	2015 EV	22.5	0.1882	2012 US136	15.9	0.1158	1.5404	-0.5235